demonstrated a significant reduction in TER119$^+$ erythroblasts in *Tie2-Cre;Tif1b*$^{fl/fl}$ fetal livers (Figure 1B). Detailed analysis revealed a block in differentiation of *Tif1b*$^{\Delta/\Delta}$ erythroblasts from CD71$^+$TER119$^-$ early erythroblasts to CD71$^+$TER119$^+$ erythroblasts (Figure S1C), resulting in a drastic reduction in the numbers of *Tif1b*$^{\Delta/\Delta}$ CD71$^+$TER119$^+$ and CD71$^-$TER119$^+$ mature erythroblasts (Figure 1C). Indeed, *Tif1b*$^{\Delta/\Delta}$ erythroblasts were mostly proerythroblasts, while the control erythroblasts were at various differentiation stages from proerythroblasts to mature erythroblasts (Figure 1D). These data are consistent with the recent reports on the impact of deletion of *Tif1b* on erythropoiesis (Barde et al., 2013), suggesting that severe anemia due to impaired erythroid differentiation could account for embryonic lethality of *Tie2-Cre;Tif1b*$^{fl/fl}$ embryos.

Of note, CD150$^+$LSK HSCs and LSK HSPCs were also significantly reduced in *Tie2-Cre;Tif1b*$^{fl/fl}$ fetal livers at E13.5 compared to the controls (Figures 1E and S1D). *Tif1b*$^{f/\Delta}$ LSK cells proliferated poorly in liquid culture compared to the control cells (Figure 1F). In colony-forming assays, *Tif1b*$^{\Delta/\Delta}$ LSK cells gave rise to significantly fewer colonies than control cells and failed to form colonies larger than 2 mm in diameter. Most of the colonies generated from *Tif1b*$^{\Delta/\Delta}$ LSK cells consisted of only neutrophils and macrophages with very few megakaryocytes but completely lacked erythroblasts (Figure 1G). We next performed competitive reconstitution assays. Not surprisingly, *Tif1b*$^{\Delta/\Delta}$ cells did not contribute to hematopoiesis in the recipient mice in either the peripheral blood (PB) or the bone marrow (BM) (Figure 1H). Further examination revealed that *Tif1b*$^{+/\Delta}$ cells also performed poorly in competitive reconstitution assays, suggesting a haploinsufficient effect with *Tif1b* heterozygotes (data not shown). Moreover, *Tif1b*$^{\Delta/\Delta}$ cells failed to extend the survival of lethally irradiated recipient mice (Figure S1E). These results indicate that loss of TIF1β severely impairs the capacity of HSCs to repopulate hematopoiesis in vivo.

### Deletion of *Tif1b* Causes BM Failure Accompanied by Depletion of HSCs

To evaluate the role of TIF1β in adult BM hematopoiesis, we next analyzed *Cre-ERT;Tif1b*$^{fl/fl}$ mice. To exclude any influences of deletion of *Tif1b* on the BM microenvironment, we first transplanted BM cells from *Cre-ERT* control and *Cre-ERT;Tif1b*$^{fl/fl}$ mice without competitor cells into lethally irradiated wild-type recipient mice. After confirming engraftment, we deleted *Tif1b* by inducing nuclear translocation of Cre with intraperitoneal injection of tamoxifen at 8 weeks after transplantation. Deletion of *Tif1b* was very efficient, with deletion efficiency in BM Lin$^-$c-KIT$^+$ progenitor cells at 92.6% by genomic quantitative PCR (data not shown). As indicated by mild reduction in BM cellularity and mild cytopenia in *Cre-ERT* control mice, tamoxifen had some toxic effects on hematopoiesis at the early time points postinjection (Figures 2B and S2A). Deletion of *Tif1b*, however, induced progressive hypoplasia of the BM and the spleen (Figures 2A and 2B) and caused obvious cytopenia in the PB (Figure S2A). Although residual Ly5.1$^+$ host cells gradually overtook *Tif1b*$^{\Delta/\Delta}$ cells and eventually restored the blood cell counts in the PB (Figures S2A and S2B), about 70% of the transplanted mice died of BM failure within 40 days of tamoxifen injection (Figure 2C).

Of interest, the number of *Tif1b*$^{\Delta/\Delta}$ HSCs increased transiently at 2 weeks postdeletion and then dramatically decreased by 4 weeks postdeletion (Figure 2D), suggesting enhanced cycling of HSCs. Indeed, 66% of the *Tif1b*$^{\Delta/\Delta}$ HSCs had exited the quiescent $G_0$ stage and a significant portion of them were actively cycling compared to the control HSCs (Figures 2E and S2C). A significant number of *Tif1b*$^{\Delta/\Delta}$ HSPCs egressed from BM to the periphery as evident from a drastic increase in LSK HSPCs and Lin$^-$c-KIT$^+$ progenitors in the PB (Figure 2F), suggesting a BM niche-interaction defect in *Tif1b*$^{\Delta/\Delta}$ HSPCs. In addition, *Tif1b*$^{\Delta/\Delta}$ HSCs underwent massive apoptosis (Figure 2G). Among the myeloid progenitors, the numbers of *Tif1b*$^{\Delta/\Delta}$ granulocyte-macrophage progenitors (GMPs) and megakaryocyte-erythroid progenitors (MEPs) were also significantly reduced at 4 weeks postdeletion (Figure S2D). Furthermore, *Tif1b*$^{\Delta/\Delta}$ LSK cells proliferated poorly in culture (Figure S2E). We next examined the long-term reconstitution capacity of *Tif1b*-deficient BM cells. To this end, control and *Cre-ERT;Tif1b*$^{fl/fl}$ BM cells were transplanted along with the same number of BM competitor cells into lethally irradiated wild-type recipients. Upon deletion of *Tif1b* at 8 weeks after transplantation, donor cells were rapidly outcompeted by the competitor cells and quickly depleted from both the PB and the BM (Figure 2H).

In contrast to its role in erythropoiesis (Barde et al., 2013), the role of TIF1β has never been tested in myeloid cells. We therefore analyzed *lysozyme-Cre;Tif1b*$^{fl/fl}$ mice, in which Cre is active only in myeloid cells at the maturation stages beyond GMPs. Surprisingly enough, *lysozyme-Cre;Tif1b*$^{fl/fl}$ mice showed no obvious defects in myeloid differentiation. The hematological data, including the PB cell counts and the lineage composition and the number of BM cells, myeloid progenitor cells and HSCs were almost normal (Figure S3). These findings underline the lineage-specific functions of TIF1β in hematopoiesis.

### Loss of HSC Signature in the Absence of TIF1β

To elucidate the changes in gene expression responsible for impaired HSC function in the absence of TIF1β, we performed microarray analysis using LSK cells at 2 weeks postdeletion of *Tif1b* (Figure 3A). The analysis revealed that 541 genes were upregulated more than 2-fold and 486 genes

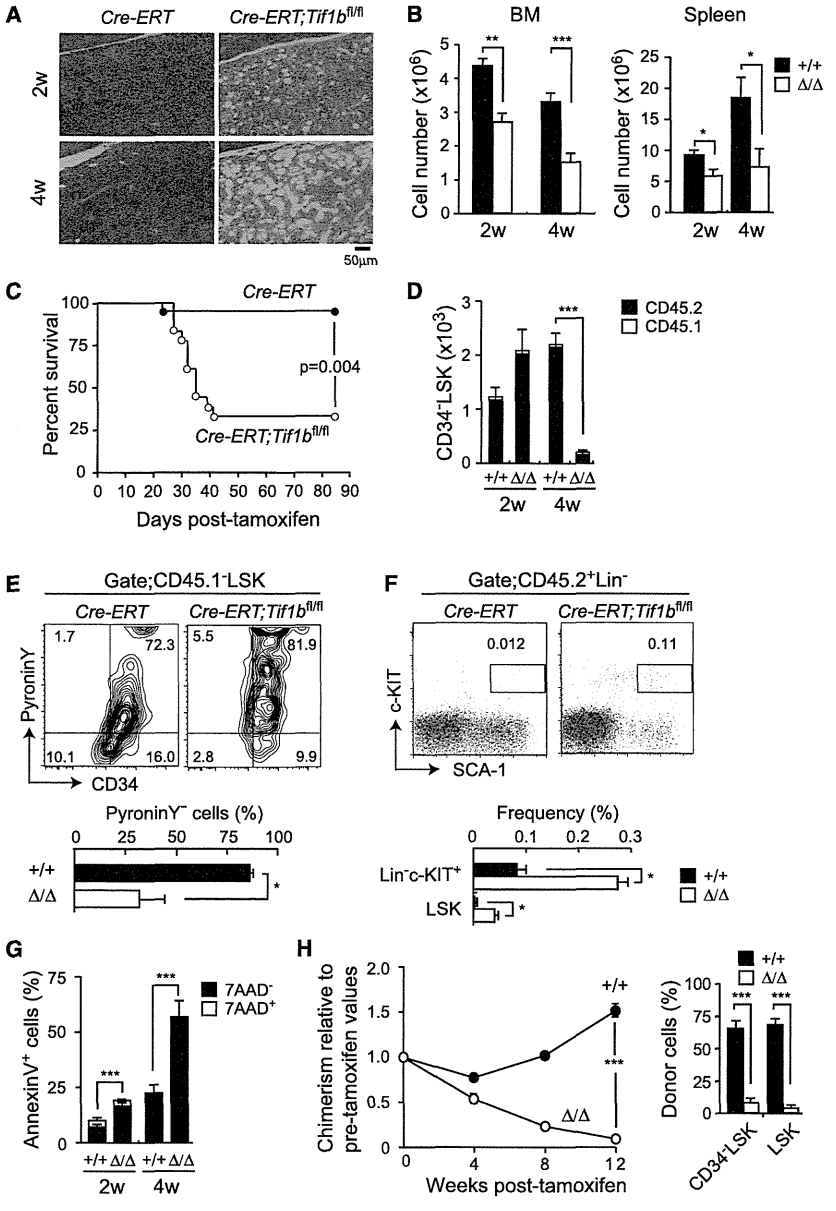


**Figure 2. Deletion of *Tif1b* Leads to Rapid BM Failure**

(A) Hematoxylin and eosin staining of BM sections from *Cre-ERT* (*Tif1b*$^{+/+}$) and *Cre-ERT;Tif1b*$^{fl/fl}$ (*Tif1b*$^{\Delta/\Delta}$) mice at 2 and 4 weeks postdeletion of *Tif1b*. BM cells from 8-week-old *Cre-ERT* and *Cre-ERT;Tif1b*$^{fl/fl}$ mice were transplanted into lethally irradiated recipient mice without competitor cells. At 8 weeks after transplantation, recipient mice were injected with tamoxifen for 5 consecutive days.

(B) Absolute numbers of total BM and spleen cells at the indicated time points postdeletion of *Tif1b* (2 weeks [2w], n = 8; 4 weeks [4w], n = 8–10).

(C) Survival curve of the recipient mice repopulated with BM cells from *Cre-ERT* and *Cre-ERT;Tif1b*$^{fl/fl}$ mice after deletion of *Tif1b* (n = 12).

(D) Absolute numbers of total *Tif1b*$^{+/+}$ and *Tif1b*$^{\Delta/\Delta}$ CD34$^-$LSK HSCs in the BM at the indicated time points after deletion of *Tif1b* (n = 8).

(E) Cell-cycle status of *Tif1b*$^{+/+}$ and *Tif1b*$^{\Delta/\Delta}$ CD34$^-$LSK HSCs determined by incorporation of Pyronin Y at 2 weeks after the first injection of tamoxifen. Representative flow cytometric profiles are depicted (upper panel) and the proportion of pyronin Y-negative cells in CD34$^-$LSK HSCs is shown as the mean ± SEM (n = 4) (lower panel).

(F) Detection of *Tif1b*$^{+/+}$ and *Tif1b*$^{\Delta/\Delta}$ HSPCs in the PB at 2 weeks after the first injection of tamoxifen. Representative flow cytometric profiles of LSK cells from *CreERT* and *CreERT;Tif1b*$^{fl/fl}$ mice are depicted (upper panel) and the proportions of Lin$^-$c-Kit$^+$ and LSK cells in total mononuclear cells is shown as the mean ± SEM (n = 4) (lower panel).

(G) Apoptosis in BM CD45.2$^+$LSK cells from recipient mice detected with Annexin V and 7-aminoactinomycin D (7-AAD) by flow cytometry at the indicated time points after deletion of *Tif1b*. The data are shown as mean ± SEM (n = 4).

(H) Competitive reconstitution assays. BM cells from 8-week-old *CreERT* and *CreERT;Tif1b*$^{fl/fl}$ mice were transplanted into lethally irradiated recipient mice with the same number of competitor BM cells (1 × 10$^6$ cells). At 8 weeks posttransplantation, recipient mice were injected with tamoxifen for 5 consecutive days. The chimerism of CD45.2$^+$ donor-derived cells in the PB of recipient mice is shown as % of chimerism values prior to treatment with tamoxifen (left panel). Donor chimerism in the BM LSK and CD34$^-$LSK cells at 12 weeks after injection of tamoxifen is also shown (right panel). The data are shown as mean ± SEM (n = 6). *p < 0.05; **p < 0.005; ***p < 0.0005.

were downregulated more than 2-fold compared to control cells reproducibly in two independent experiments. We first performed gene set enrichment analysis (GSEA) to see if there was a fundamental loss of stem-cell-like gene expression in *Tif1b*$^{\Delta/\Delta}$ HSCs. Using the microarray data taken from various hematopoietic compartments (CD34$^-$LSK HSCs, CD34$^+$LSK MPPs, Lin$^-$c-KIT$^+$ committed progenitors, and Lin$^+$ differentiated cells), we found that a gene signature unique to CD34$^-$LSK HSCs was actually enriched in *Tif1b*$^{\Delta/\Delta}$LSKs (Figure 3B). This suggests that a loss

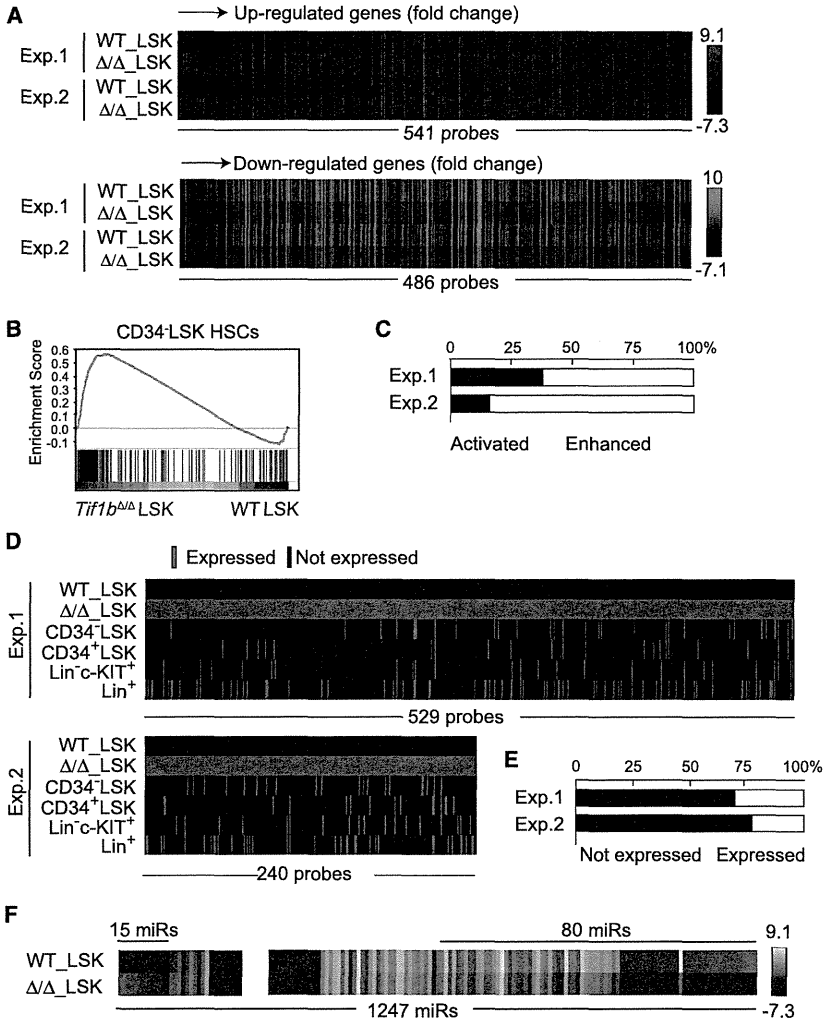


**Figure 3. Derepression of Nonhematopoietic Genes in *Tif1b*-Deficient LSK Cells**

(A) Heatmap of the expression of genes that were upregulated (541 probe sets, upper panel) or downregulated (486 probe sets, lower panel) more than 2-fold in *Tif1b*-deficient BM LSK cells in the microarray analysis.

(B) GSEA of the gene set specific to CD34$^-$LSK HSCs in *Tif1b*$^{\Delta/\Delta}$ LSK cells. Using the microarray data from CD34$^-$LSK HSCs, CD34$^+$LSK MPPs, Lin$^-$c-KIT$^+$ committed progenitors, and Lin$^+$ differentiated cells, HSC-specific gene sets were selected and applied to GSEA.

(C) Upregulated genes in (A) were divided into two groups according to their expression levels in *Tif1b*$^{\Delta/\Delta}$ LSK cells compared to that in control LSK cells. One group consist of probe sets that were expressed in the control LSK cells and their expression levels were enhanced upon deletion of *Tif1b* ("enhanced" genes). The other group includes probe sets that were not expressed in the control LSK cells but became activated in *Tif1b*-deficient LSK cells ("activated" genes). Bar graph shows proportions of these groups.

(D) Schematic representation of expression profiles of "Activated" genes in BM *Tif1b*-deficient LSK cells in (A) in various hematopoietic cell fractions, including CD34$^-$LSK HSCs, CD34$^+$LSK MPPs, Lin$^-$c-KIT$^+$ committed progenitors, and Lin$^+$ differentiated cells. Expressed genes are depicted as a red bar.

(E) Proportions of probe sets in (D) that were not expressed in any of the hematopoietic cell fractions (Not expressed) and those expressed in at least one of the hematopoietic cell fractions including CD34$^-$LSK HSCs, CD34$^+$LSK MPPs, Lin$^-$c-KIT$^+$ committed progenitors and Lin$^+$ differentiated cells (Expressed).

(F) Heatmap of the expression of miRNAs that were upregulated (15 miRs) or downregulated (80 miRs) more than 2-fold in *Tif1b*-deficient BM LSK cells in the microarray analysis.

of "stemness" is not responsible for the phenotypes observed in *Tif1b*-deficient mice.

We next focused on the genes derepressed in the absence of TIF1β. Among genes derepressed, a significant portion of genes became transcriptionally detectable from undetectable levels ("activated") in *Tif1b*$^{\Delta/\Delta}$ LSK cells (Figure 3C). We then compared the expression profiles of the "activated" genes in *Tif1b*$^{\Delta/\Delta}$ BM LSK cells to various hematopoietic compartments, including CD34$^-$LSK HSCs, CD34$^+$LSK MPPs, Lin$^-$c-KIT$^+$ committed progenitors, and Lin$^+$ differentiated cells (Figure 3D). To our surprise, the majority of "activated" gene transcripts were not detected in any of these hematopoietic compartments (Figure 3E). These results suggest that TIF1β is required for the gene silencing of nonhematopoietic genes in HSPCs.

Among gene sets positively enriched (derepressed) in *Tif1b*$^{\Delta/\Delta}$ LSK cells, many genes sets were related to signaling pathways mediated by cell surface receptors or adhesion molecules (e.g., integrin signaling pathway, gap junction, and focal adhesion; see Table S1) and upregulation of such genes was confirmed by quantitative RT-PCR (Figure S4A). These results indicate deregulated expression of nonhematopoietic adhesion molecules in *Tif1b*$^{\Delta/\Delta}$ HSCs, which might result in impaired niche interaction in *Tif1b*$^{\Delta/\Delta}$ HSCs and enhanced egression of HSCs from the BM to the periphery.

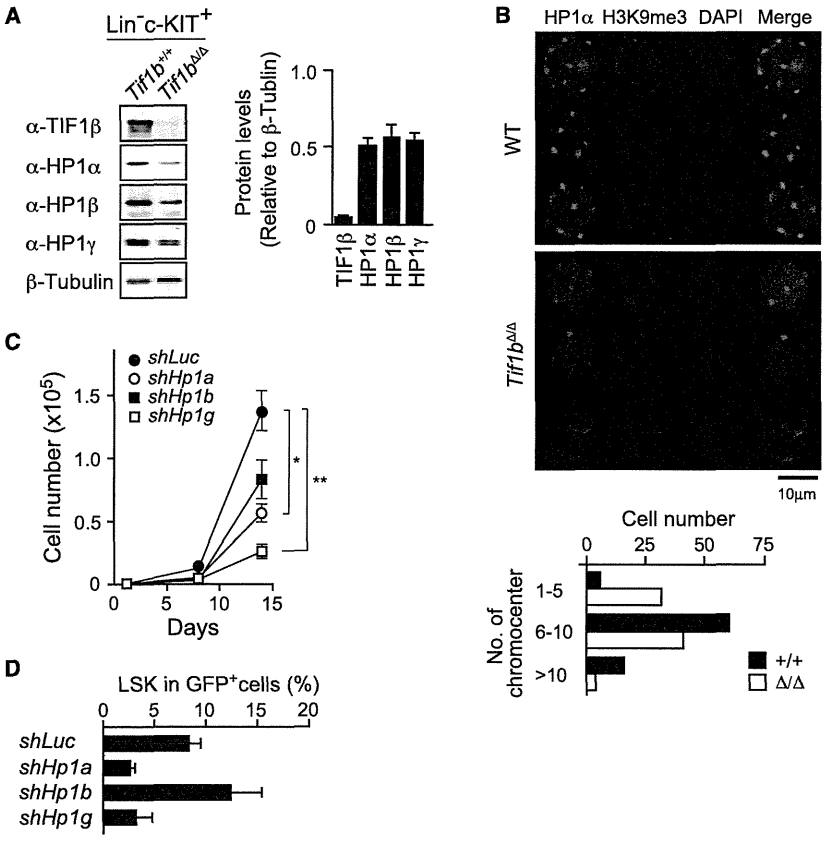


**Figure 4. HP1 Depletion Compromises the Proliferation of HSCs**

(A) Western blot analysis of Lin⁻c-Kit⁺ fetal liver cells from *Tie2-Cre* and *Tie2-Cre;Tif1b*$^{fl/fl}$ embryos. Levels of HP1 proteins were normalized to the amount of β-tubulin. The relative levels of HP1 proteins are indicated in the right panel. The data are shown as mean ± SEM (n = 3).

(B) Immunostaining of HP1α and H3K9me3 in LSK cells from *Tie2-Cre* and *Tie2-Cre; Tif1b*$^{fl/fl}$ fetal livers at E13.5. Cells were counterstained with DAPI. Representative three individual cell images are depicted. Numbers of chromocenters per cell are shown in the bottom panel. In total, 100 cells were counted for the scoring of the chromocenters.

(C) Growth of CD34⁻KSL HSCs upon depletion of *Hp1* genes in vitro. HSCs were transduced with lentiviruses generating shRNAs against *Luciferase* (*Luc*), *Hp1a*, *Hp1b*, and *Hp1g* and then allowed to proliferate in the presence of 100 ng/ml of SCF and TPO for 14 days. The transduction efficiency was around 75% in most experiments as judged from the GFP expression. The data are shown as mean ± SEM for triplicate cultures.

(D) Analysis of CD34⁻KSL HSC cultures depleted of *Hp1* genes in (C) at day 14. The proportion of LSK cells in GFP⁺ cells is shown. The data are shown as mean ± SEM (n = 3).

Barde et al. (2013) have recently reported that deletion of *Tif1b* results in compromised erythropoiesis due to failure in the induction of mitophagy-related genes. They found that the TIF1β together with KRAB-ZNF represses the transcription of microRNAs (miRNAs) targeting mitophagy transcripts to induce mitophagy during the terminal differentiation of erythroblasts. Profiling of miRNAs in *Tif1b*$^{\Delta/\Delta}$ LSK cells revealed upregulation of 15 miRNA greater than 2-fold compared to control cells (Figure 3F). However, none of the mitophagy-related miRNAs described by Barde et al. were upregulated in *Tif1b*$^{\Delta/\Delta}$ LSK cells. In addition, the expression levels of mitophagy-related genes were not significantly altered in *Tif1b*$^{\Delta/\Delta}$ LSK cells (data not shown). Together, these findings highlight the cell-type-specific as well as differentiation stage-specific functions of TIF1β in hematopoiesis. Nonetheless, it should be noted that some of the upregulated miRNAs potentially target genes downregulated in *Tif1b*$^{\Delta/\Delta}$ LSK cells, implying involvement of derepressed miRNAs in altered gene expression in *Tif1b*$^{\Delta/\Delta}$ LSK cells (data not shown).

TIF1β has been characterized to suppress activation of p53 (Tian et al., 2009). Indeed, p53 target genes, such as proapoptotic genes *Bax*, *Noxa*, and *p21*, were upregulated in fetal *Tif1b*$^{\Delta/\Delta}$ LSK cells (Figure S4B). In order to evaluate the contribution of p53, we transplanted *Cre-ERT;Tif1b*$^{fl/fl}$ CD34⁻LSK HSCs transduced with the E6 oncoprotein, a potent p53 inhibitor, into lethally irradiated recipients. E6, however, did not have any gross effects on the repopulating capacity of *Tif1b*$^{\Delta/\Delta}$ HSCs (Figure S4C), suggesting that the activated p53 response is not the causative event in the hematopoietic failure induced by absence of TIF1β.

### Reduction in HP1 Proteins in the Absence of TIF1β

TIF1β physically interacts with all of the HP1 proteins (HP1α, HP1β, and HP1γ; Nielsen et al., 1999; Cammas et al., 2002, 2007) and recruits them in order to establish deep silencing of their target genes (Nielsen et al., 1999; Schultz et al., 2002). Notably, levels of all three members of the HP1 family proteins were reduced approximately 2-fold in fetal liver *Tif1b*$^{\Delta/\Delta}$ Lin⁻c-KIT⁺ progenitor cells (Figure 4A), though their transcription levels were not significantly changed (data not shown). In accordance with this finding, immunostaining of fetal liver LSK cells revealed a reduction in numbers of chromocenters, a structural

component of heterochromatin where HP1α accumulates, in the absence of TIF1β (Figure 4B). These results support the notion that TIF1β functions as a scaffold that stabilizes HP1 proteins. The level of HP1α protein was significantly reduced also in NIH 3T3 cells depleted of TIF1β. However, inhibition of proteasome activity by MG132 in NIH cells failed to stabilize HP1α upon knockdown of *Tif1b*, leaving the molecular mechanism through which the HP1 proteins are destabilized in the absence of TIF1β still obscure (data not shown). HP1 proteins are recruited to their target loci via physical interaction with TIF1β as well as through direct binding to trimethylated H3K9 to form transcriptionally inactive heterochromatin (Nestorov et al., 2013). The levels of global histone modifications, including H3K9me1/2/3, did not significantly change in $Tif1b^{\Delta/\Delta}$ $Lin^{-}c\text{-}KIT^{+}$ progenitor cells (Figure S4D). These findings further suggest that TIF1β regulates HP1 function not only by tethering them to their targets but also by securing their posttranslational stability. In order to test whether the reduction in levels of HP1 proteins is involved in the impaired function of $Tif1b^{\Delta/\Delta}$ HSCs, we knocked down the *Hp1* genes in HSCs using small hairpin RNAs (shRNAs) (Figure S4E). Growth of HSCs was significantly impaired upon depletion of *Hp1a* and *Hp1g*, but not *Hp1b* (Figure 4C). The proportion of LSK HSPCs in $GFP^{+}$ transduced cells was also significantly decreased upon depletion of *Hp1a* and *Hp1g*, but not *Hp1b*, at day 14 of culture (Figure 4D). These results suggest that reduced levels of HP1 proteins play a role in determining the phenotypes of *Tif1b*-deficient HSCs. Together, our findings highlight the TIF1β-HP1 system as critical transcriptional machinery that keeps nonhematopoietic genes repressed in HSCs, thereby maintaining the transcriptional signature specific to HSCs.

TIF1β has been reported to repress the expression of endogenous retrotransposons in embryonic stem cells via the histone methyltransferase ESET/SETDB1 and subsequent H3K9 trimethylation (Matsui et al., 2010; Rowe et al., 2010). However, we did not observe any significant derepression of endogenous retrotransposons in $Tif1b^{\Delta/\Delta}$ LSK cells (data not shown), indicating that different silencing machineries are operating in embryonic stem cells and somatic stem cells. Of interest, the phenotypes of $Tif1b^{\Delta/\Delta}$ HSCs are similar to those of HSCs deficient for MI-2β, a component of the NuRD histone deacetylase complex, which directly interacts with TIF1β (Schultz et al., 2001; Yoshida et al., 2008). TIF1β may thus collaborate with the NuRD complex, in addition to HP1 proteins, and stabilize these repressor molecules critical for the transcriptional repression of nonhematopoietic genes in HSCs.

The epigenetic regulation of transcription is crucial for the maintenance of cell-type-specific signatures (Sashida and Iwama, 2012). In the point of view of transcriptional regulation, multipotency of stem cells can be defined as an ability of stem cells to express a set of genes required for differentiation and cell-type-specific function upon cell differentiation. The PcG proteins maintain this "transcriptional competence" by transiently silencing genes that will be activated during differentiation of stem cells (Sauvageau and Sauvageau, 2010). In contrast, our findings in this study indicate that the TIF1β-HP1 system, which collaborates with H3K9me3 and DNA methylation (Rowe et al., 2013), is involved in establishing a more stable silencing state of genes that would never be activated in a given cell lineage. However, the precise mechanisms by which the epigenetic switching between the reversible PcG-mediated system and the TIF1β-HP1 system that we propose here remain to be elucidated. Understanding how these different repressive systems work would prove invaluable to our understanding of the epigenetic regulation of stem cells.

## EXPERIMENTAL PROCEDURES

Details regarding experimental procedures are available in Supplemental Experimental Procedures.

### ACCESSION NUMBERS

Microarray data have been deposited in the NCBI Gene Expression Omnibus with the accession numbers GSE48929, GSE48986, and GSE52282.

### SUPPLEMENTAL INFORMATION

Supplemental Information includes Supplemental Experimental Procedures, four figures, and one table and can be found with this article online at http://dx.doi.org/10.1016/j.stemcr.2013.12.008.

### ACKNOWLEDGMENTS

We thank Drs. P. Chambon and R. Losson for providing $Tif1b^{fl/fl}$ mice and Dr. Nozaki (MAB institute) for modified histone antibodies. This work was supported in part by Grants-in-Aid for Scientific Research (grants 21390289 and 22180002) and Scientific Research on Innovative Areas "Cell Fate" (grant 22118004) from MEXT (Japan) and by a Grant-in-Aid for Core Research for Evolutional Science and Technology (CREST) from the Japan Science and Technology Corporation (JST).

Received: July 12, 2013
Revised: December 11, 2013
Accepted: December 12, 2013
Published: January 23, 2014

### REFERENCES

Barde, I., Rauwel, B., Marin-Florez, R.M., Corsinotti, A., Laurenti, E., Verp, S., Offner, S., Marquis, J., Kapopoulou, A., Vanicek, J., and Trono, D. (2013). A KRAB/KAP1-miRNA cascade regulates

erythropoiesis through stage-specific control of mitophagy. Science *340*, 350–353.

Cammas, F., Mark, M., Dollé, P., Dierich, A., Chambon, P., and Losson, R. (2000). Mice lacking the transcriptional corepressor TIF1beta are defective in early postimplantation development. Development *127*, 2955–2963.

Cammas, F., Oulad-Abdelghani, M., Vonesch, J.L., Huss-Garcia, Y., Chambon, P., and Losson, R. (2002). Cell differentiation induces TIF1beta association with centromeric heterochromatin via an HP1 interaction. J. Cell Sci. *115*, 3439–3448.

Cammas, F., Janoshazi, A., Lerouge, T., and Losson, R. (2007). Dynamic and selective interactions of the transcriptional corepressor TIF1 beta with the heterochromatin protein HP1 isotypes during cell differentiation. Differentiation *75*, 627–637.

Chikuma, S., Suita, N., Okazaki, I.M., Shibayama, S., and Honjo, T. (2012). TRIM28 prevents autoinflammatory T cell development in vivo. Nat. Immunol. *13*, 596–603.

Matsui, T., Leung, D., Miyashita, H., Maksakova, I.A., Miyachi, H., Kimura, H., Tachibana, M., Lorincz, M.C., and Shinkai, Y. (2010). Proviral silencing in embryonic stem cells requires the histone methyltransferase ESET. Nature *464*, 927–931.

Nestorov, P., Tardat, M., and Peters, A.H. (2013). H3K9/HP1 and Polycomb: two key epigenetic silencing pathways for gene regulation and embryo development. Curr. Top. Dev. Biol. *104*, 243–291.

Nielsen, A.L., Ortiz, J.A., You, J., Oulad-Abdelghani, M., Khechumian, R., Gansmuller, A., Chambon, P., and Losson, R. (1999). Interaction with members of the heterochromatin protein 1 (HP1) family and histone deacetylation are differentially involved in transcriptional silencing by members of the TIF1 family. EMBO J. *18*, 6385–6395.

Oguro, H., Yuan, J., Ichikawa, H., Ikawa, T., Yamazaki, S., Kawamoto, H., Nakauchi, H., and Iwama, A. (2010). Poised lineage specification in multipotential hematopoietic stem and progenitor cells by the polycomb protein Bmi1. Cell Stem Cell *6*, 279–286.

Rowe, H.M., Jakobsson, J., Mesnard, D., Rougemont, J., Reynard, S., Aktas, T., Maillard, P.V., Layard-Liesching, H., Verp, S., Marquis, J., et al. (2010). KAP1 controls endogenous retroviruses in embryonic stem cells. Nature *463*, 237–240.

Rowe, H.M., Friedli, M., Offner, S., Verp, S., Mesnard, D., Marquis, J., Aktas, T., and Trono, D. (2013). De novo DNA methylation of endogenous retroviruses is shaped by KRAB-ZFPs/KAP1 and ESET. Development *140*, 519–529.

Sashida, G., and Iwama, A. (2012). Epigenetic regulation of hematopoiesis. Int. J. Hematol. *96*, 405–412.

Sauvageau, M., and Sauvageau, G. (2010). Polycomb group proteins: multi-faceted regulators of somatic stem cells and cancer. Cell Stem Cell *7*, 299–313.

Schultz, D.C., Friedman, J.R., and Rauscher, F.J., 3rd. (2001). Targeting histone deacetylase complexes via KRAB-zinc finger proteins: the PHD and bromodomains of KAP-1 form a cooperative unit that recruits a novel isoform of the Mi-2α subunit of NuRD. Genes Dev. *15*, 428–443.

Schultz, D.C., Ayyanathan, K., Negorev, D., Maul, G.G., and Rauscher, F.J., 3rd. (2002). SETDB1: a novel KAP-1-associated histone H3, lysine 9-specific methyltransferase that contributes to HP1-mediated silencing of euchromatic genes by KRAB zinc-finger proteins. Genes Dev. *16*, 919–932.

Tian, C., Xing, G., Xie, P., Lu, K., Nie, J., Wang, J., Li, L., Gao, M., Zhang, L., and He, F. (2009). KRAB-type zinc-finger protein Apak specifically regulates p53-dependent apoptosis. Nat. Cell Biol. *11*, 580–591.

Yoshida, T., Hazan, I., Zhang, J., Ng, S.Y., Naito, T., Snippert, H.J., Heller, E.J., Qi, X., Lawton, L.N., Williams, C.J., and Georgopoulos, K. (2008). The role of the chromatin remodeler Mi-2β in hematopoietic stem cell self-renewal and multilineage differentiation. Genes Dev. *2*, 1174–1189.

Published November 11, 2013

JEM

Article

# Concurrent loss of *Ezh2* and *Tet2* cooperates in the pathogenesis of myelodysplastic disorders

Tomoya Muto,[1,2,3] Goro Sashida,[1,4] Motohiko Oshima,[1,4] George R. Wendt,[1,10] Makiko Mochizuki-Kashio,[1,4] Yasunobu Nagata,[5] Masashi Sanada,[5] Satoru Miyagi,[1,4] Atsunori Saraya,[1,4] Asuka Kamio,[6] Genta Nagae,[6] Chiaki Nakaseko,[2,3] Koutaro Yokote,[2] Kazuya Shimoda,[7] Haruhiko Koseki,[4,8] Yutaka Suzuki,[9] Sumio Sugano,[9] Hiroyuki Aburatani,[6] Seishi Ogawa,[5] and Atsushi Iwama[1,4]

[1]Department of Cellular and Molecular Medicine and [2]Department of Clinical Cell Biology and Medicine, Graduate School of Medicine, Chiba University, Chiba 260-8670, Japan
[3]Department of Hematology, Chiba University Hospital, Chiba 260-8670, Japan
[4]Japan Science and Technology Corporation (JST), Core Research for Evolutional Science and Technology (CREST), Gobancho, Chiyoda-ku, Tokyo 102-0076, Japan
[5]Cancer Genomics Project, Graduate School of Medicine, University of Tokyo, Tokyo 113-8655, Japan
[6]Genome Science Division, Research Center for Advanced Science and Technology, University of Tokyo, Tokyo 153-8904, Japan
[7]Department of Gastroenterology and Hematology, Faculty of Medicine, Miyazaki University, Miyazaki 889-1692, Japan
[8]Laboratory for Lymphocyte Development, RIKEN Center for Integrative Medical Sciences, Yokohama 230-0045, Japan
[9]Laboratory of Functional Genomics, Department of Medical Genome Sciences, Graduate School of Frontier Sciences, University of Tokyo, Chiba 277-8562, Japan
[10]ITO Foundation for International Education Exchange, Shinjuku 160-0023, Japan

**Polycomb group (PcG) proteins are essential regulators of hematopoietic stem cells. Recent extensive mutation analyses of the myeloid malignancies have revealed that inactivating somatic mutations in PcG genes such as *EZH2* and *ASXL1* occur frequently in patients with myelodysplastic disorders including myelodysplastic syndromes (MDSs) and MDS/myeloproliferative neoplasm (MPN) overlap disorders (MDS/MPN). In our patient cohort, *EZH2* mutations were also found and often coincided with *tet methylcytosine dioxygenase 2* (*TET2*) mutations. Consistent with these findings, deletion of *Ezh2* alone was enough to induce MDS/MPN-like diseases in mice. Furthermore, concurrent depletion of *Ezh2* and *Tet2* established more advanced myelodysplasia and markedly accelerated the development of myelodysplastic disorders including both MDS and MDS/MPN. Comprehensive genome-wide analyses in hematopoietic progenitor cells revealed that upon deletion of *Ezh2*, key developmental regulator genes were kept transcriptionally repressed, suggesting compensation by Ezh1, whereas a cohort of oncogenic direct and indirect polycomb targets became derepressed. Our findings provide the first evidence of the tumor suppressor function of EZH2 in myeloid malignancies and highlight the cooperative effect of concurrent gene mutations in the pathogenesis of myelodysplastic disorders.**

Recent genomic studies have identified a series of recurrent somatic mutations in patients with myeloid malignancies, including myelodysplastic syndrome (MDS), myeloproliferative neoplasm (MPN), chronic myelomonocytic leukemia (CMML)—classified as an MDS/MPN—and acute myeloid leukemia (AML). Notably, these mutations frequently occur in epigenetic regulator genes such as *tet methylcytosine dioxygenase 2* (*TET2*), *isocitrate dehydrogenase 1* (*IDH1*), *IDH2*, *DNA methyltransferase 3A* (*DNMT3A*), and polycomb group (PcG) genes (Chung et al., 2012; Raza and Galili, 2012; Shih et al., 2012). PcG proteins form the polycomb repressive complexes (PRCs) 1 and 2. PRC2 contains three core subunits: SUZ12, one of the EED isoforms, and the histone methyltransferase EZH1 or EZH2, which

CORRESPONDENCE
Atsushi Iwama:
aiwama@faculty.chiba-u.jp

Abbreviations used: AML, acute myeloid leukemia; AML/MRC, AML with myelodysplasia-related changes; ChIP-seq, chromatin immunoprecipitation sequencing; CMML, chronic myelomonocytic leukemia; *DNMT3A*, *DNA methyltransferase 3A*; ES, embryonic stem; GMP, granulocyte-macrophage progenitor; GSEA, gene set enrichment analysis; HSC, hematopoietic stem cell; *IDH1*, *isocitrate dehydrogenase 1*; MDS, myelodysplastic syndrome; MPN, myeloproliferative neoplasm; MPP, multipotent progenitor cell; PcG, polycomb group; PRC, polycomb repressive complex; RefSeq, Reference Sequence; TET2, tet methylcytosine dioxygenase 2; TSS, transcriptional start site.

T. Muto, G. Sashida, and M. Oshima contributed equally to this paper.



The Rockefeller University Press $30.00
J. Exp. Med. 2013 Vol. 210 No. 12 2627-2639
www.jem.org/cgi/doi/10.1084/jem.20131144

Supplemental Material can be found at:
http://jem.rupress.org/content/suppl/2013/11/08/jem.20131144.DC1.html

Published November 11, 2013



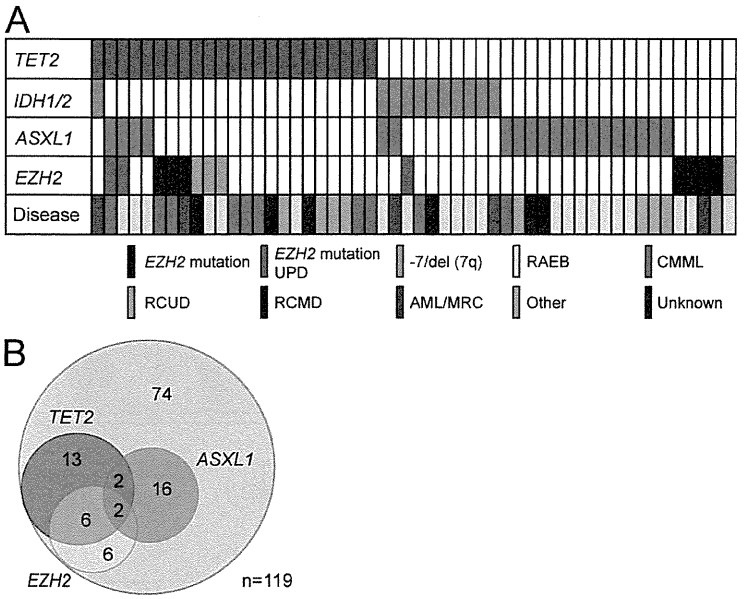


**Figure 1. Distribution of mutations in epigenetic regulator genes in patients with myelodysplastic disorders.** (A) Mutations of *TET2*, *IDH1/2*, *EZH2*, and *ASXL1* in 52 samples from 119 patients with MDS, CMML, and AML/MRC shown by colored bars. Each column represents 1 of the 52 samples with a mutation in one or more of the genes listed. *EZH2* mutations include uniparental disomy (UPD) of *EZH* mutation and deletion of *EZH2* (located at 7q36) associated with -7 and 7q- chromosomal abnormalities. The disease types of these 52 patients are also shown. Refractory anemia with excess blasts (RAEB) includes RAEB-1 and RAEB-2. CMML includes CMML-1 and CMML-2. RCUD and RCMD denote Refractory cytopenia with unilineage or multilineage dysplasia, respectively. Other diseases include 5q- syndrome, Refractory anemia with ring sideroblasts (RARS), and MDS, unclassifiable (MDS-U). (B) Venn diagrams showing the number of patients who have both *TET2* and PcG mutations. The overlap between mutations in *TET2* and *EZH2* is statistically significant ($P < 0.001$).

catalyzes di- and tri-methylation of histone H3 at lysine 27 (H3K27me3). Canonical PRC1 contains four core subunits, PCGF (which can include BMI1 or MEL18), CBX, PHC, and RING1A or RING1B, which monoubiquitylates histone H2A at lysine 119 (H2AK119ub1). PRC1 and PRC2 cooperatively function as transcriptional repressors via establishing these repressive histone modifications. PcG genes have been implicated in the maintenance of self-renewing somatic and cancer stem cells (Konuma et al., 2010; Sauvageau and Sauvageau, 2010) and have typically been characterized as oncogenes, as exemplified by somatic activating mutations of *EZH2* in follicular and diffuse large B cell lymphomas (Morin et al., 2010). However, *EZH2*, which is located at chromosome 7q36, is frequently involved in chromosomal abnormalities such as -7 and 7q-, and inactivating mutations of *EZH2* have also been identified in patients with MDS, MPN, and CMML—all clonal myeloid disorders originating from hematopoietic stem cells (HSCs; Ernst et al., 2010; Nikoloski et al., 2010). Of interest, other components of PRC2, *EED*, and *SUZ12* appeared to be mutated in a manner similar to *EZH2*, although the frequencies of their mutations are much lower than those of *EZH2* mutations. The PRC2-related gene *ASXL1*, which plays an important role in the recruitment and/or stability of PRC2 (Abdel-Wahab et al., 2012), has also been shown to carry inactivating mutations in patients with MDS, MPN, and CMML (Abdel-Wahab et al., 2011; Bejar et al., 2011).

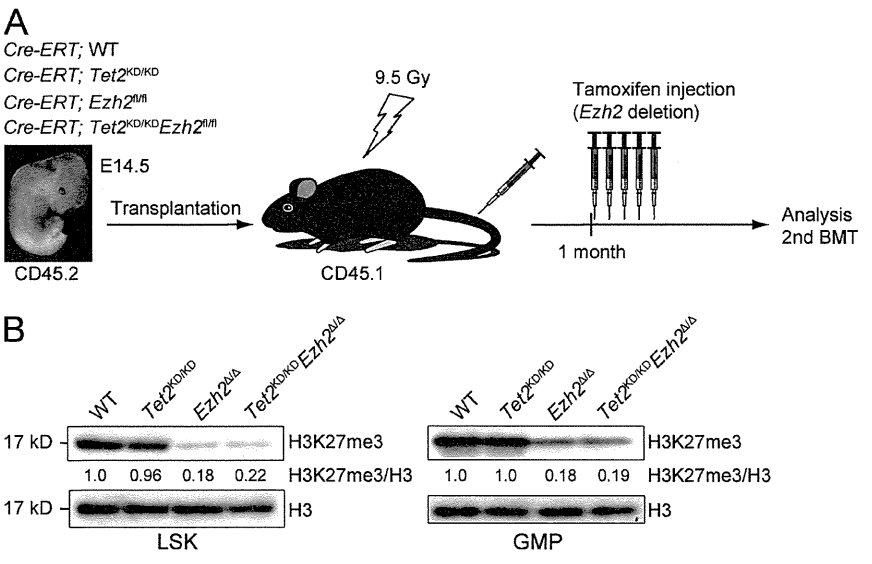


**Figure 2. Generation of mice reconstituted with *Tet2*$^{KD/KD}$, *Ezh2*$^{\Delta/\Delta}$, and *Tet2*$^{KD/KD}$*Ezh2*$^{\Delta/\Delta}$ hematopoietic cells.** (A) A schematic diagram of the experimental process. $10^6$ E14.5 fetal liver cells from *Cre-ERT*;WT, *Cre-ERT;Tet2*$^{KD/KD}$, *Cre-ERT;Ezh2*$^{fl/fl}$, and *Cre-ERT;Tet2*$^{KD/KD}$*Ezh2*$^{fl/fl}$ CD45.2 mice were transplanted into lethally irradiated CD45.1 recipient mice. For deletion of *Ezh2*, 100 µl tamoxifen (10 mg/ml) was intraperitoneally injected once a day for 5 consecutive days at 4 wk after transplantation. (B) Levels of H3K27me3 in LSK cells and GMPs. LSK cells and GMPs from BM of WT, *Tet2*$^{KD/KD}$, *Ezh2*$^{\Delta/\Delta}$, and *Tet2*$^{KD/KD}$*Ezh2*$^{\Delta/\Delta}$ mice were analyzed by Western blotting using an anti-H3K27me3 antibody at 4 mo after transplantation. Levels of H3K27me3 were normalized to the amount of H3 and are indicated relative to WT control values. The levels of H3K27me3 in WT cells were arbitrarily set to 1. The representative data from two independent experiments are presented.

Published November 11, 2013



Although these mutations suggest a tumor suppressor function of PRC2-related genes in these diseases, both the impact of each PcG mutation and its interplay with coinciding mutations remain largely unknown.

Loss-of-function mouse models of *Tet2*, *Dnmt3a*, and *Bap1*, as well as gain-of-function mouse models of *IDH1*, have been reported to recapitulate some aspects of malignancies (Moran-Crusio et al., 2011; Challen et al., 2012; Dey et al., 2012; Sasaki et al., 2012). However, the role of PcG-related mutants has not yet been tested in mice. To understand the contribution of inactivating PcG mutations to the development of myeloid malignancies, we examined the *Ezh2*-deficient mice over longer periods of time and also tested the impact of concurrent depletion of *Ezh2* and *Tet2* on hematopoiesis.

## RESULTS

### Somatic mutations of PcG genes in myeloid dysplasia

In our cohort of 119 patients with myelodysplastic disorders, which includes MDS, CMML, and AML with myelodysplasia-related changes (AML/MRC), inactivating mutations in *EZH2* and *ASXL1* were detected in 8.4 and 16.8% of patients, respectively. Moreover, 3.4% of patients had deletion of *EZH2* (located at 7q36) associated with -7 and 7q- chromosomal abnormalities (Fig. 1 A and Table S1). Notably, 57.1% of these *EZH2* mutations coexisted with *TET2* mutations. Conversely, 34.8% of patients with *TET2* mutations had coexisting *EZH2* mutations (Fig. 1 B). These findings suggest a link between *EZH2* and *TET2* mutations in the pathogenesis of myelodysplastic disorders.

### Deletion of *Ezh2* results in enhanced repopulating capacity of HSCs and promotes myeloid-biased repopulation

To decipher the pathological role of inactivating *EZH2* mutations and concurrent inactivation of *EZH2* and *TET2* genes in malignant stem cell disorders, we crossed *Cre-ERT;Ezh2*$^{fl/fl}$ mice (Mochizuki-Kashio et al., 2011) and *Tet2* gene trap mice (*Tet2*$^{KD/KD}$; Shide et al., 2012). *Tet2*$^{KD/KD}$ mice, in which the gene trap vector is inserted into exon 2 of *Tet2* just before the first coding exon, express *Tet2* mRNA at levels ~20% of those of the WT mice and frequently die by postnatal day 3 (Shide et al., 2012). Considering the early death of *Tet2*$^{KD/KD}$ mice and a necessity to exclude the influence of the loss of *Tet2* and *Ezh2* in BM niche cells, we transplanted E14.5 fetal liver cells from *Cre-ERT* control (WT), *Cre-ERT;Tet2*$^{KD/KD}$, *Cre-ERT;Ezh2*$^{fl/fl}$, and *Cre-ERT;Tet2*$^{KD/KD}$*Ezh2*$^{fl/fl}$ CD45.2 mice into lethally irradiated CD45.1 recipient mice and deleted *Ezh2* by intraperitoneal injection of tamoxifen at 4 wk after transplantation (Fig. 2 A). We hereafter refer to the recipient mice reconstituted with *Tet2*$^{KD/KD}$, *Ezh2*$^{\Delta/\Delta}$, and *Tet2*$^{KD/KD}$*Ezh2*$^{\Delta/\Delta}$ cells as *Tet2*$^{KD/KD}$, *Ezh2*$^{\Delta/\Delta}$, and *Tet2*$^{KD/KD}$*Ezh2*$^{\Delta/\Delta}$ mice, respectively. EZH2 is a catalytic component of PRC2 that catalyzes the methylation of H3K27. As expected, the levels of H3K27me3 were markedly reduced upon deletion of *Ezh2* in both Lineage$^-$Sca-1$^+$c-Kit$^+$ (LSK) cells, which include HSCs and multipotent progenitor cells (MPPs), and in granulocyte-macrophage progenitors (GMPs; Fig. 2 B). TET2, a methylcytosine dioxygenase, catalyzes the oxidation of 5-mC (5-methylcytosine) to 5-hmC (5-hydroxymethyl cytosine), the first step of active demethylation ((Ernst et al., 2010; Ko et al., 2010). The levels of 5-hmC in total BM cells were also reduced in *Tet2*$^{KD/KD}$ and *Tet2*$^{KD/KD}$*Ezh2*$^{\Delta/\Delta}$ cells, whereas there was no obvious

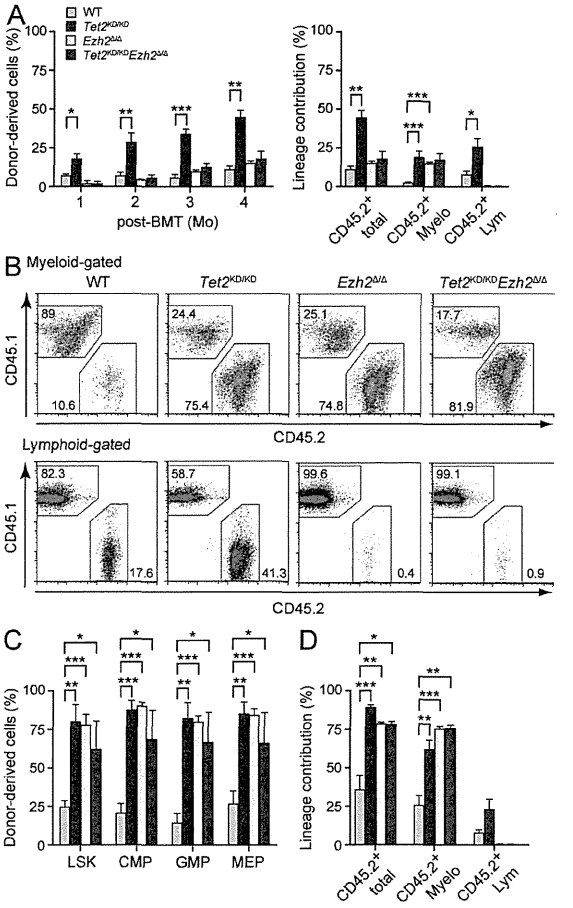


**Figure 3. Enhanced repopulating capacity of *Tet2*$^{KD/KD}$, *Ezh2*$^{\Delta/\Delta}$, and *Tet2*$^{KD/KD}$*Ezh2*$^{\Delta/\Delta}$ HSCs.** (A) Competitive repopulating assays. 600 LSK cells from WT, *Tet2*$^{KD/KD}$, *Ezh2*$^{\Delta/\Delta}$, and *Tet2*$^{KD/KD}$*Ezh2*$^{\Delta/\Delta}$ mice at 12 wk after deletion of *Ezh2* were injected into lethally irradiated CD45.1 recipients with 4 × 10$^5$ CD45.1 competitor BM cells. The percentages of donor-derived total CD45.2$^+$ hematopoietic cells in the PB (left) and the percentages of total CD45.2$^+$ hematopoietic cells and myeloid (Gr-1$^+$ and/or Mac-1$^+$) and lymphoid (B220$^+$, CD4$^+$, or CD8$^+$) cells in the PB at 12 wk after transplantation (right) are shown as mean ± SEM ($n$ = 4–6). These data are representative data from two independent experiments. (B) Representative flow cytometric profiles of donor-derived CD45.2$^+$ myeloid (top) and lymphoid cells (bottom) in the PB at 12 wk after transplantation. (C) Percentages of donor-derived CD45.2$^+$ hematopoietic cells in the BM LSK HSC/MPP and myeloid progenitor fractions. The data are shown as mean ± SEM ($n$ = 4–6). (D) Secondary transplantation assays. Total BM cells (2 × 10$^6$) from primary recipient mice at 12 wk after transplantation were transplanted into lethally irradiated recipient mice without competitor cells. The percentages of donor-derived total CD45.2$^+$ hematopoietic cells and myeloid and lymphoid cells in the PB at 20 wk after transplantation are shown as mean ± SEM ($n$ = 3–5). *, $P < 0.05$; **, $P < 0.01$; ***, $P < 0.001$.

Published November 11, 2013



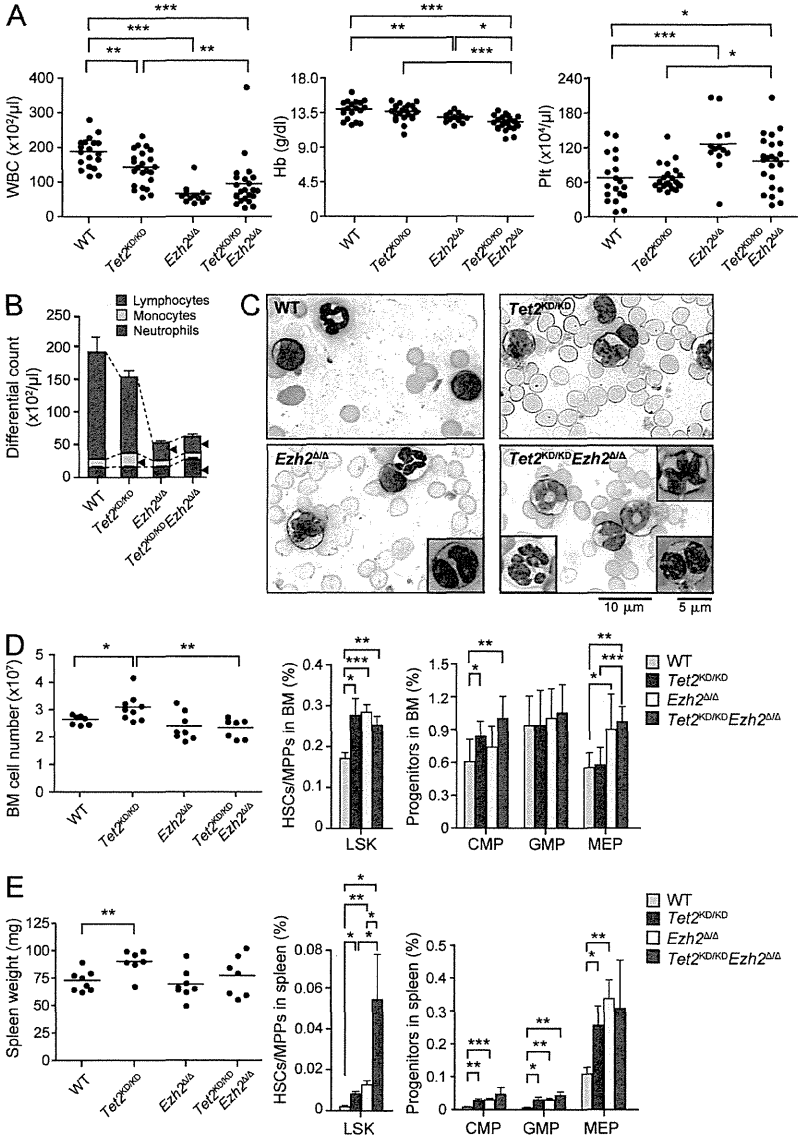


**Figure 4. Hematopoiesis in the recipient mice reconstituted with *Tet2*$^{KD/KD}$, *Ezh2*$^{\Delta/\Delta}$, and *Tet2*$^{KD/KD}$ *Ezh2*$^{\Delta/\Delta}$ hematopoietic cells.** (A) PB cell counts in recipients reconstituted with *Tet2*$^{KD/KD}$, *Ezh2*$^{\Delta/\Delta}$, and *Tet2*$^{KD/KD}$*Ezh2*$^{\Delta/\Delta}$ fetal liver hematopoietic cells at 12 wk after deletion of *Ezh2*. White blood cell (WBC), hemoglobin (Hb), and platelet (Plt) counts in the PB from WT ($n = 19$), *Tet2*$^{KD/KD}$ ($n = 23$), *Ezh2*$^{\Delta/\Delta}$ ($n = 13$), and *Tet2*$^{KD/KD}$*Ezh2*$^{\Delta/\Delta}$ ($n = 23$) mice are plotted as dots and the mean values are indicated as bars. (B) The hematopoietic compartment of the PB assessed by manual differential cell counts, performed at 12 wk after deletion of *Ezh2*. WT ($n = 5$), *Tet2*$^{KD/KD}$ ($n = 7$), *Ezh2*$^{\Delta/\Delta}$ ($n = 5$), and *Tet2*$^{KD/KD}$*Ezh2*$^{\Delta/\Delta}$ ($n = 6$) mice are represented as mean ± SEM. Arrowheads indicate statistically significant populations compared with WT ($P < 0.05$). (C) Smear preparation of PB from WT, *Tet2*$^{KD/KD}$, *Ezh2*$^{\Delta/\Delta}$, and *Tet2*$^{KD/KD}$*Ezh2*$^{\Delta/\Delta}$ mice at 12 wk after deletion of *Ezh2* observed after May-Giemsa staining. Bar, 10 μm. Hyposegmented neutrophils consistent with a pseudo Pelger-Huët anomaly (bottom right), hypersegmented neutrophils (bottom left), and dysplastic monocyte (top right) are depicted in insets. Bar, 5 μm. (D) BM analysis of WT, *Tet2*$^{KD/KD}$, *Ezh2*$^{\Delta/\Delta}$, and *Tet2*$^{KD/KD}$*Ezh2*$^{\Delta/\Delta}$ mice at 12 wk after deletion of *Ezh2*. Absolute numbers of total BM cells from a unilateral pair of the femur and the tibia of WT ($n = 7$), *Tet2*$^{KD/KD}$ ($n = 9$), *Ezh2*$^{\Delta/\Delta}$ ($n = 8$), and *Tet2*$^{KD/KD}$*Ezh2*$^{\Delta/\Delta}$ mice ($n = 7$) are plotted as dots and mean values are indicated as bars (left). The percentage of LSK cells (middle) and myeloid progenitors (right) are presented as mean ± SEM (WT, $n = 7$; *Tet2*$^{KD/KD}$, $n = 6$; *Ezh2*$^{\Delta/\Delta}$, $n = 6$; *Tet2*$^{KD/KD}$*Ezh2*$^{\Delta/\Delta}$, $n = 6$). (E) Extramedullary hematopoiesis in the spleen of *Tet2*$^{KD/KD}$, *Ezh2*$^{\Delta/\Delta}$, and *Tet2*$^{KD/KD}$*Ezh2*$^{\Delta/\Delta}$ mice at 12 wk after deletion of *Ezh2*. Spleen weights of WT ($n = 8$), *Tet2*$^{KD/KD}$ ($n = 7$), *Ezh2*$^{\Delta/\Delta}$ ($n = 8$), and *Tet2*$^{KD/KD}$*Ezh2*$^{\Delta/\Delta}$ mice ($n = 7$) are plotted as dots and mean values are indicated as bars (left). Percentage of LSK cells (middle) and myeloid progenitors (right) are presented as mean ± SEM (WT, $n = 5$; *Tet2*$^{KD/KD}$, $n = 5$; *Ezh2*$^{\Delta/\Delta}$, $n = 7$; *Tet2*$^{KD/KD}$*Ezh2*$^{\Delta/\Delta}$, $n = 4$). *, $P < 0.05$; **, $P < 0.01$; ***, $P < 0.001$.

difference in the levels of 5-mC among each genotype (unpublished data).

To explore the consequence of loss of Ezh2 and/or Tet2 in hematopoietic stem/progenitor cells, we first performed competitive repopulating assays using LSK cells recovered from the recipient mice at 3 mo after deletion of *Ezh2*. It has been reported that Tet2 loss leads to increased HSC self-renewal and myeloid transformation (Moran-Crusio et al., 2011; Shide et al., 2012). As expected, *Tet2*$^{KD/KD}$ LSK cells readily established progressively increasing chimerism in the PB over time (Fig. 3 A). Similarly, the contribution of *Ezh2*$^{\Delta/\Delta}$ and *Tet2*$^{KD/KD}$ *Ezh2*$^{\Delta/\Delta}$ LSK-derived cells to the myeloid compartment of the PB increased over time, although the total chimerism was lower than that of *Tet2*$^{KD/KD}$ cells because of inefficient production of lymphocytes by *Ezh2*-deficient LSK cells (Fig. 3, A and B). Indeed, LSK cells of all genotypes established significantly higher chimerism in the BM LSK fraction compared with WT LSK cells (Fig. 3 C). All mutant cells taken from the primary recipients continued to propagate in the secondary recipients during serial transplantation and exhibited myeloid-biased differentiation (Fig. 3 D). These results reveal that the loss of Ezh2 augments the repopulating capacity of HSCs and activates the production of myeloid cells in much the same way as the loss of Tet2 does.

### Deletion of *Ezh2* causes myeloid dysplasia in mice

We next analyzed the hematopoiesis in recipient mice reconstituted with *Tet2*$^{KD/KD}$, *Ezh2*$^{\Delta/\Delta}$, and *Tet2*$^{KD/KD}$*Ezh2*$^{\Delta/\Delta}$ cells. PB from *Ezh2*$^{\Delta/\Delta}$ and *Tet2*$^{KD/KD}$*Ezh2*$^{\Delta/\Delta}$ mice at 3 mo after deletion of *Ezh2* showed reduced white blood cell counts due to lymphopenia and increased platelet counts. In addition, mild but significant anemia was detected in these mice (Fig. 4, A and B).

Published November 11, 2013



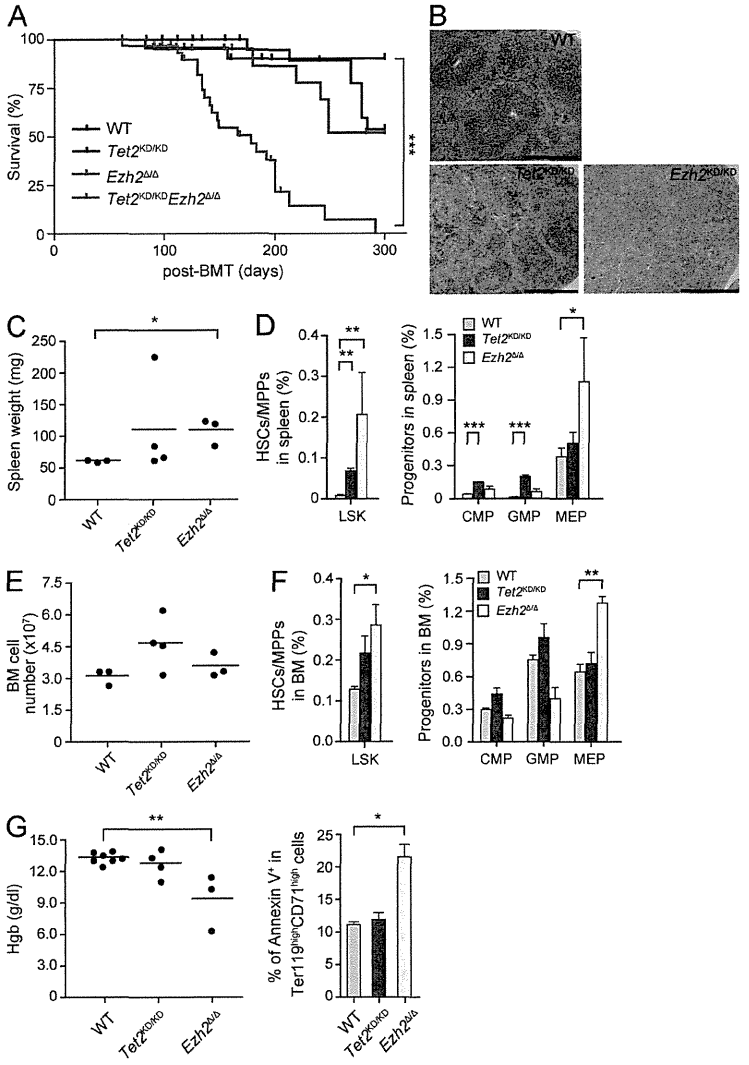


**Figure 5. *Ezh2*$^{\Delta/\Delta}$ mice develop myelodysplastic disorders.** (A) Kaplan-Meier survival curve of WT ($n$ = 24), *Tet2*$^{KD/KD}$ ($n$ = 28), *Ezh2*$^{\Delta/\Delta}$ ($n$ = 23), and *Tet2*$^{KD/KD}$*Ezh2*$^{\Delta/\Delta}$ ($n$ = 32) mice. Some of the mice (WT, $n$ = 11; *Tet2*$^{KD/KD}$, $n$ = 11; *Ezh2*$^{\Delta/\Delta}$, $n$ = 11; *Tet2*$^{KD/KD}$*Ezh2*$^{\Delta/\Delta}$, $n$ = 13) were sacrificed for analyses in the middle of observation (indicated by short vertical bars on the curves). These survival curves were generated from two to four independent experiments. n.s., not significant. (B) Hematoxylin and Eosin (H&E) staining of paraffin-embedded sections of spleen. Bars, 500 µm. (C) Spleen weights plotted as dots with the mean values indicated as bars (WT, $n$ = 3; *Tet2*$^{KD/KD}$, $n$ = 4; and *Ezh2*$^{\Delta/\Delta}$, $n$ = 3). (D) The percentage of LSK cells and myeloid progenitors in the spleen presented as mean ± SEM (WT, $n$ = 5; *Tet2*$^{KD/KD}$, $n$ = 4; and *Ezh2*$^{\Delta/\Delta}$, $n$ = 3). (E) Absolute numbers of total BM cells from a unilateral pair of the femur and the tibia are plotted as dots and mean values are indicated as bars. (F) Percentage of LSK cells and myeloid progenitors in the BM presented as mean ± SEM. The numbers of mice analyzed are WT, $n$ = 3; *Tet2*$^{KD/KD}$, $n$ = 4; and *Ezh2*$^{\Delta/\Delta}$, $n$ = 3. (G) Hemoglobin contents in PB are plotted as dots and mean values are indicated as bars (left). Percentage of Annexin V$^+$ cells in Ter119$^{high}$CD71$^{high}$ BM erythroblasts is also shown as mean ± SEM from three independent experiments. The numbers of mice analyzed are WT, $n$ = 3; *Tet2*$^{KD/KD}$, $n$ = 3; and *Ezh2*$^{\Delta/\Delta}$, $n$ = 3 (right). *, $P < 0.05$; **, $P < 0.01$; ***, $P < 0.001$.

*Tet2*$^{KD/KD}$ mice showed monocytosis in PB as reported previously (Moran-Crusio et al., 2011), whereas *Tet2*$^{KD/KD}$*Ezh2*$^{\Delta/\Delta}$ mice did not (Fig. 4 B). Cytological analysis of *Ezh2*$^{\Delta/\Delta}$ and *Tet2*$^{KD/KD}$*Ezh2*$^{\Delta/\Delta}$ PB revealed morphological abnormalities in myeloid cells, such as delayed maturation of neutrophils, hyposegmented neutrophils consistent with a pseudo Pelger-Huët anomaly, hypersegmented neutrophils, and dysplasia of monocytes (Fig. 4 C). This trend was more evident in *Tet2*$^{KD/KD}$ *Ezh2*$^{\Delta/\Delta}$ PB compared with *Ezh2*$^{\Delta/\Delta}$ PB but was not obvious in *Tet2*$^{KD/KD}$ PB (Fig. 4 C).

BM analysis at 3 mo after deletion of *Ezh2* revealed that although total BM cell numbers were mildly increased only in *Tet2*$^{KD/KD}$ mice, all mutant mice had a greater proportion of LSK cells than the WT mice (Fig. 4 D). Similarly, *Tet2*$^{KD/KD}$, *Ezh2*$^{\Delta/\Delta}$, and *Tet2*$^{KD/KD}$*Ezh2*$^{\Delta/\Delta}$ mice had a greater proportion of common myeloid progenitors (CMPs) and/or MEPs (Fig. 4 D). Furthermore, extramedullary hematopoiesis was evident in the spleen of all mutant mice as defined by a significant increase in the absolute number of LSK cells and myeloid progenitors, although splenomegaly was evident only in *Tet2*$^{KD/KD}$ mice, likely because of impaired lymphopoiesis in the absence of Ezh2 (Fig. 4 E).

### *Ezh2*$^{\Delta/\Delta}$ and *Tet2*$^{KD/KD}$*Ezh2*$^{\Delta/\Delta}$ mice develop myelodysplastic disorders

During a long observation period, we found that not only *Tet2*$^{KD/KD}$ mice but also *Ezh2*$^{\Delta/\Delta}$ mice die of hematological disorders. This is the first study to describe the lethal hematologic phenotypes caused by loss of Ezh2. *Tet2*$^{KD/KD}$ mice developed CMML-like disease accompanied by monocytosis and extramedullary hematopoiesis as reported previously (Moran-Crusio et al., 2011) and half of the mice died by 10 mo after transplantation. Notably, *Ezh2*$^{\Delta/\Delta}$ mice also developed MDS/MPN-like disease and half of the mice died by 10 mo after transplantation (Fig. 5 A and Table S2). They showed myeloproliferative features characterized by active extramedullary

Published November 11, 2013



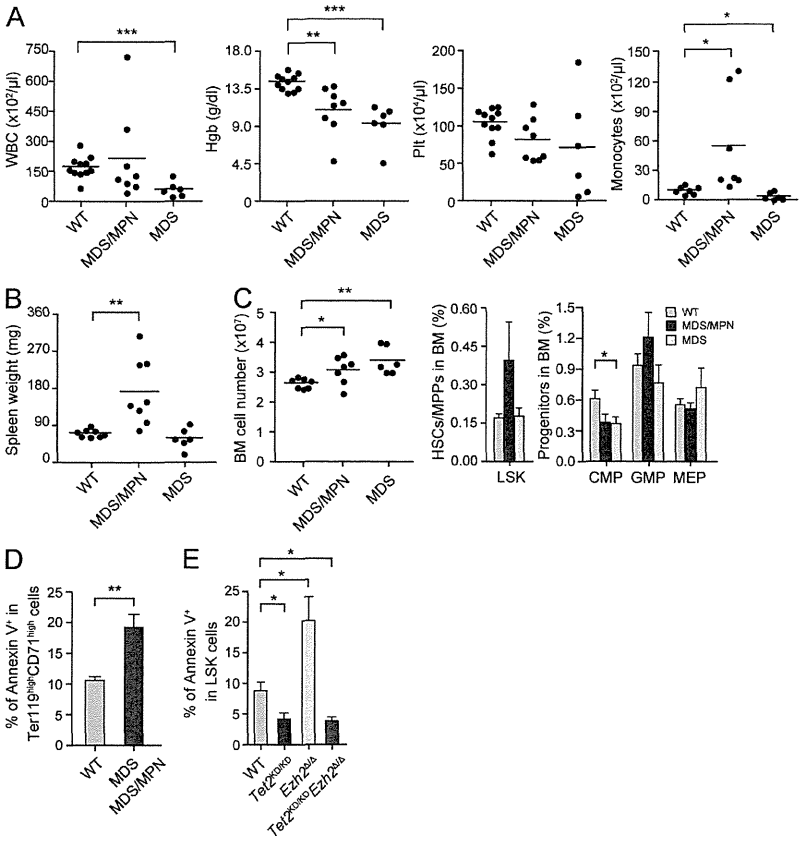


**Figure 6. *Tet2*$^{KD/KD}$*Ezh2*$^{\Delta/\Delta}$ mice develop myelodysplastic disorders.** (A–C) Hematological data from moribund *Tet2*$^{KD/KD}$*Ezh2*$^{\Delta/\Delta}$ mice and those surviving at 300 d after transplantation. PB cell counts and the number of monocytes in the PB (A), spleen weights (B), and absolute numbers of total BM cells from a unilateral pair of the femur and the tibia (C, left) are plotted as dots and mean values are indicated as bars. Percentage of LSK cells (C, middle) and myeloid progenitor cells (C, right) are presented as mean ± SEM. Data were collected from WT ($n$ = 8), MDS/MPN ($n$ = 8), and MDS ($n$ = 6) mice for spleen weights and WT ($n$ = 11), MDS/MPN ($n$ = 7), and MDS ($n$ = 6) mice for others. (D) Percentage of Annexin V$^+$ cells in Ter119$^{high}$CD71$^{high}$ BM erythroblasts shown as mean ± SEM from three independent experiments (WT, $n$ = 3; MDS/MPN, $n$ = 2; MDS, $n$ = 2). (E) Percentage of Annexin V$^+$ cells in LSK cells from the indicated mice at 8 mo after transplantation shown as mean ± SEM from three independent experiments (WT, $n$ = 3; *Tet2*$^{KD/KD}$, $n$ = 3; *Ezh2*$^{\Delta/\Delta}$, $n$ = 3; and *Tet2*$^{KD/KD}$*Ezh2*$^{\Delta/\Delta}$, $n$ = 3). *, P < 0.05; **, P < 0.01; ***, P < 0.001.

hematopoiesis in the spleen as evident from splenomegaly with a marked increase in LSK cells and MEPs resulting in effacement of lymphoid follicles (Fig. 5, B–D). They also showed a significant increase in LSK cells and MEPs in the BM, whereas they did not show obvious monocytosis in the PB (Fig. 5, E and F; and Table S2). They were anemic and showed increased apoptosis in Ter119$^{high}$CD71$^{high}$ erythroblasts (Fig. 5 G) and LSK cells (Fig. 6 E) in the BM, suggesting ineffective erythropoiesis, a feature compatible with myelodysplastic disorders. *Ezh2*$^{\Delta/\Delta}$ mice also showed dysplasia of myeloid cells as described above (Fig. 4 C).

To our surprise, concurrent deletion of *Tet2* and *Ezh2* significantly shortened the latency of disease development and all *Tet2*$^{KD/KD}$*Ezh2*$^{\Delta/\Delta}$ mice died by 10 mo after transplantation (Fig. 5 A). Histological analysis of moribund *Tet2*$^{KD/KD}$*Ezh2*$^{\Delta/\Delta}$ mice revealed lethal pneumonia in all mice analyzed ($n$ = 6; unpublished data). *Tet2*$^{KD/KD}$*Ezh2*$^{\Delta/\Delta}$ mice developed heterogeneous diseases which were classified into two types of myeloid neoplasms: (1) MDS/MPN including CMML ($n$ = 8) and (2) MDS ($n$ = 6; Table S2). MDS/MPN mice showed myeloproliferative features, including CMML-like monocytosis in the PB (Fig. 6 A and Table S2) and/or splenomegaly with extramedullary hematopoiesis (Fig. 6 B), and an increase in LSK cells in the BM (Fig. 6 C). In contrast, MDS mice did not show obvious myeloproliferative features but showed a trend of pancytopenia (Fig. 6 A and Table S2). Myeloid dysplasia, including delayed maturation of neutrophils, a pseudo Pelger-Huët anomaly, hypersegmented neutrophils, and dysplasia of monocytes, was evident in *Tet2*$^{KD/KD}$*Ezh2*$^{\Delta/\Delta}$ mice compared with *Tet2*$^{\Delta/\Delta}$ and *Ezh2*$^{\Delta/\Delta}$ mice as described above (Fig. 4 C). Furthermore, MDS and MDS/MPN mice had a lower proportion of Ter119$^+$ erythroblasts compared with WT mice (unpublished data). The proportion of Annexin V$^+$ cells in CD71$^{high}$ Ter119$^{high}$ erythroblasts was significantly higher in both MDS and MDS/MPN mice compared with their WT counterparts, implicating enhanced apoptosis as a cause of anemia (Fig. 6 D). In contrast, enhanced apoptosis in the absence of Ezh2 was canceled by loss of Tet2 in LSK cells at 8 mo after transplantation (Fig. 6 E), suggesting differential impact of loss of Ezh2 and Tet2 on apoptosis in disease-initiating cells.

## Alterations in expression of Ezh1 target genes associated with disease progression

To elucidate the changes in gene expression responsible for the hematological phenotypes induced by loss of Ezh2 and/or Tet2, we performed microarray analysis using LSK cells and GMPs from each mutant mouse at 3 mo after deletion of *Ezh2* and MDS/MPN and MDS mice. Of interest, there was significant overlap between genes up-regulated or down-regulated in *Tet2*$^{KD/KD}$ and *Ezh2*$^{\Delta/\Delta}$ LSK cells. This was true among all genotypes and diseases, and the overall gene expression profiles were highly correlated with each other (Fig. 7). To better

Published November 11, 2013



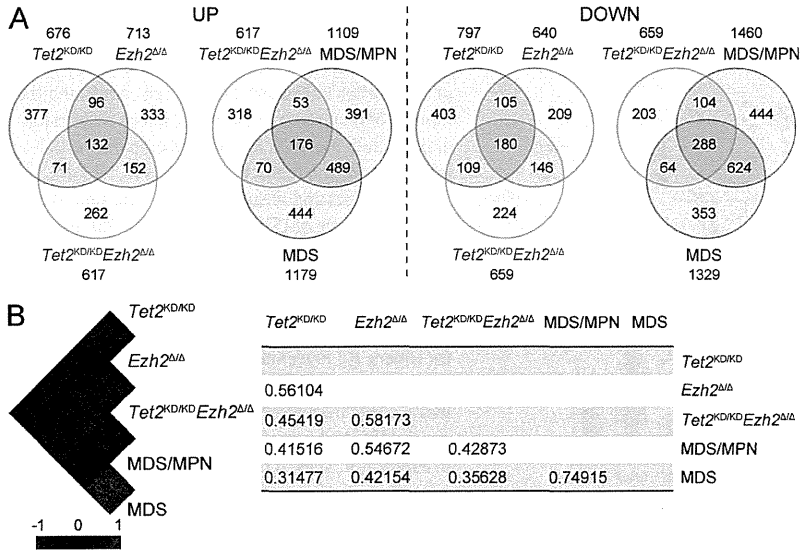


**Figure 7. Gene expression alterations associated with disease progression.** (A) Venn diagram of genes up-regulated or down-regulated in LSK cells from *Tet2*$^{KD/KD}$, *Ezh2*$^{\Delta/\Delta}$, and *Tet2*$^{KD/KD}$*Ezh2*$^{\Delta/\Delta}$ mice at 4 mo after transplantation and MDS/MPN (ID19) and MDS (ID18) mice (>2.0- or <0.5-fold compared with the WT control, respectively). The numbers of genes in each group are indicated. The overlaps between every two gene sets are statistically significant ($P < 0.01$). (B) A heat map showing the correlation of overall gene expression profiles among LSK cells from the indicated mice. Black, red, and blue colors represent no, positive, and negative correlation, respectively. The score of correlation coefficient between LSK cells from each genotype or diseased mice was defined with Pearson's correlation and is shown on the right.

understand the consequences of the loss of Ezh2 and/or Tet2, we next performed gene set enrichment analysis (GSEA; Subramanian et al., 2005). Embryonic stem (ES) cell–like signatures, which have been widely used in assessment of cancer gene signatures, are subdivided into a PRC module, a Myc module, and a core ES module (Kim et al., 2010). Among these, the Myc module, which is active in various cancers and predicts cancer outcome, was significantly enriched in *Ezh2*$^{\Delta/\Delta}$ LSK cells and became highly enriched in *Tet2*$^{KD/KD}$*Ezh2*$^{\Delta/\Delta}$ LSK cells during the development of MDS/MPN and MDS (Fig. 8 A). Of note, the Myc module became enriched in LSK cells but not in GMPs, suggesting the existence of pathological stem cells in the LSK fraction. Several modules related to enhanced cell cycle were also positively enriched in MDS/MPN and MDS LSK cells (unpublished data). We next analyzed gene sets of Ezh2 targets that lose H3K27me3 upon deletion of *Ezh2* in ES cells (ES_Ezh2 targets) and Ezh1 targets profiled in *Ezh2*$^{-/-}$ ES cells (ES_Ezh1 targets; Shen et al., 2008). As expected, all of the PRC2 gene sets showed a trend of positive enrichment (derepression) in *Ezh2*$^{\Delta/\Delta}$ and *Tet2*$^{KD/KD}$*Ezh2*$^{\Delta/\Delta}$ LSK cells and GMPs (Fig. 8 A). Notably, however, Ezh1 targets were negatively enriched (repressed) and the degree of positive enrichment of Ezh2 targets was attenuated in *Tet2*$^{KD/KD}$*Ezh2*$^{\Delta/\Delta}$ LSK cells from mice which developed myelodysplastic disorders. These data suggest compensatory action by Ezh1 in LSK cells during the development of myelodysplastic disorders. Of interest, both the Ezh1 and Ezh2 targets were positively enriched even in *Tet2*$^{KD/KD}$ LSK cells, suggesting some involvement of Tet2 in PRC2-mediated gene silencing in HSC/MPPs.

### Alterations in H3K27me3 upon deletion of Ezh2

To assess the genome-wide effects of loss of Ezh2 and/or Tet2 on epigenome, we conducted chromatin immunoprecipitation sequencing (ChIP-seq) for H3K27me3 in hematopoietic cells from WT, *Tet2*$^{KD/KD}$, *Ezh2*$^{\Delta/\Delta}$, and *Tet2*$^{KD/KD}$*Ezh2*$^{\Delta/\Delta}$ mice at 4 mo after transplantation. Due to the paucity of LSK HSC/MPPs, we used GMPs for ChIP-seq analysis and characterized the H3K27me3 levels over the region from 5.0 kb upstream to 0.5 kb downstream of transcriptional start sites (TSSs) of Reference Sequence (RefSeq) genes (Pruitt et al., 2007). As expected, drastic reductions in the levels of H3K27me3 were observed in GMPs from *Ezh2*$^{\Delta/\Delta}$ and *Tet2*$^{KD/KD}$*Ezh2*$^{\Delta/\Delta}$ mice, although considerable levels of H3K27me3 remained even in the absence of Ezh2 (Fig. 8 B). Among PcG targets (greater than fourfold enrichment of H3K27me3 compared with input in WT GMPs) that showed greater than twofold reduction of H3K27me3 levels in *Tet2*$^{KD/KD}$*Ezh2*$^{\Delta/\Delta}$ GMPs, 121 genes were derepressed greater than twofold in both MDS/MPN and MDS LSK cells compared with WT. These genes included 24 potential oncogenes such as *Hmga2* (Oguro et al., 2012), *Pbx3* (Li et al., 2013), and *Lmo1* (Tremblay et al., 2010; Table S3).

Surprisingly, H3K27me3 marks around TSSs became more enriched (greater than onefold compared with WT) in a small portion of genes upon deletion of *Ezh2*, particularly in *Ezh2*$^{\Delta/\Delta}$ GMPs (Fig. 8, B–D), suggesting a major role for Ezh1 on these gene promoters. Indeed, these genes overlapped considerably with the targets of Ezh1 in ES cells (Shen et al., 2008; Fig. 8 E), and this trend was more obvious with genes that showed high levels of H3K27me3 (>35-fold enrichment of H3K27me3 compared with input in *Ezh2*$^{\Delta/\Delta}$ GMPs). More importantly, the genes that maintained H3K27me3 levels upon deletion of *Ezh2* were overlapped markedly with genes marked with bivalent histone domains in ES cells (Bernstein et al., 2006; Ku et al., 2008; Fig. 8 F). This trend was again more obvious with the 124 genes that showed high levels of H3K27me3 (>35-fold enrichment of H3K27me3 in *Ezh2*$^{\Delta/\Delta}$ GMPs), and most of these genes appeared to be canonical developmental regulators, including genes encoding homeobox, paired-box, T-box, forkhead, and Gata family transcription factors and zinc finger DNA-binding proteins (Table S4). Because the amounts of DNA immunoprecipitated from *Ezh2*$^{\Delta/\Delta}$ and *Tet2*$^{KD/KD}$ *Ezh2*$^{\Delta/\Delta}$ GMPs are less than those from WT and *Tet2*$^{KD/KD}$ GMPs, we

Published November 11, 2013



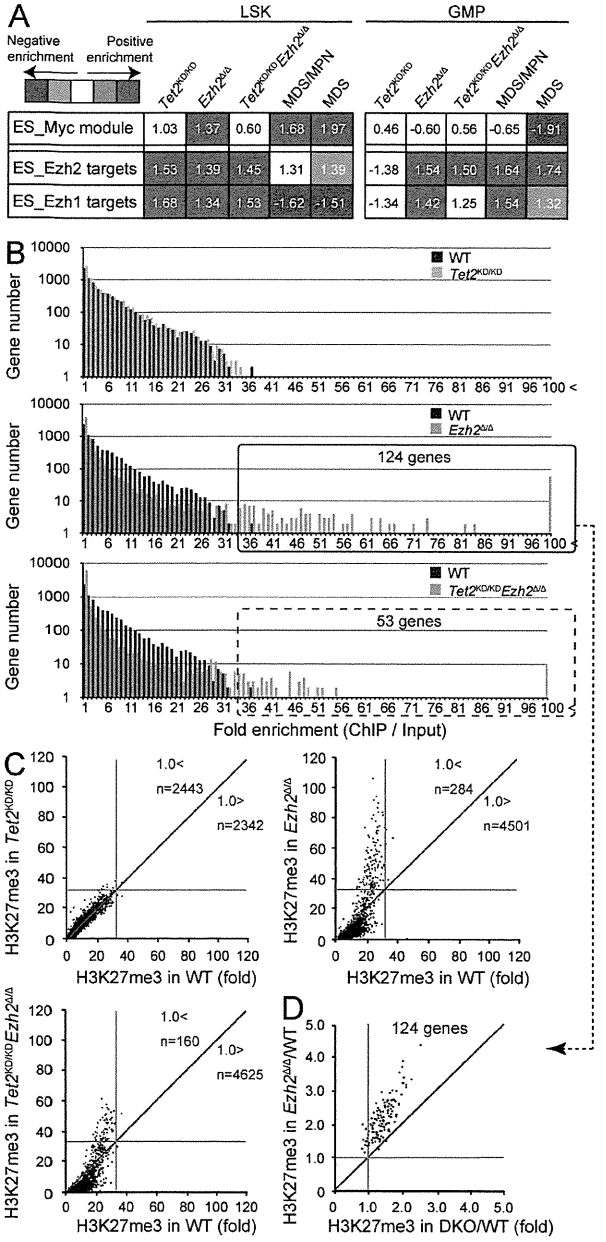


**Figure 8. Alterations in gene expression and H3K27me3 levels upon deletion of *Ezh2*.** (A) Gene expression alterations associated with disease progression. Normalized enrichment score (NES) from overall gene expression profiles of LSK cells and GMPs derived from GSEA is shown as the number in each cell. Red and blue colors represent positive (up-regulated in the given genotype relative to WT) and negative (up-regulated in WT relative to the given genotype) enrichment, respectively. Concentrated colors show that the nominal p-value is <0.05 and false discovery rate (FDR) is <0.05, which suggests meaningful enrichment for the given gene sets. Pale colors show borderline enrichment. The cells which do not meet these criteria show white color. (B) Summary of H3K27me3 enrichment detected by ChIP-seq analysis. GMPs isolated from primary recipient mice at 4 mo after transplantation were subjected to ChIP-seq analysis using an anti-H3K27me3 antibody. The fold enrichment values of H3K27me3 signals were calculated against the input signals (ChIP/input) from 5.0 kb upstream to 0.5 kb downstream of the TSSs of RefSeq genes. The red boxes indicate genes with the H3K27me3 enrichment >35-fold in $Ezh2^{\Delta/\Delta}$ and $Tet2^{KD/KD}Ezh2^{\Delta/\Delta}$ GMPs. (C) Scatter plots of H3K27me3 enrichment in $Tet2^{KD/KD}$, $Ezh2^{\Delta/\Delta}$, and $Tet2^{KD/KD}Ezh2^{\Delta/\Delta}$ GMPs in comparison with that in WT GMPs. Gray lines indicate 35-fold enrichment, which is the value defined as high enrichment in A. The numbers of genes with higher and lower fold enrichment than that of WT (divided by red lines) are indicated. (D) Scatter plots of 124 genes enclosed by a red square in B showing the H3K27me3 enrichment >35-fold relative to WT in $Ezh2^{\Delta/\Delta}$ and $Tet2^{KD/KD}Ezh2^{\Delta/\Delta}$ (DKO) GMPs. Gray lines indicate 1.0, which is the value indicating that $Ezh2^{\Delta/\Delta}$ and $Tet2^{KD/KD}Ezh2^{\Delta/\Delta}$ GMPs showed the same fold enrichment as WT. (E and F) The proportion of Ezh1 target genes (E) and genes that are marked with univalent (H3K4me3 or H3K27me3) or bivalent histone domains (H3K4me3 and H3K27me3; F) identified in ES cells were categorized by the changes in H3K27me3 levels in $Ezh2^{\Delta/\Delta}$ GMPs. The proportions in all RefSeq genes are shown in the first lane. PRC2 target genes were subdivided into genes with reduced H3K27me3 levels (<0.5-fold compared with WT), genes that maintained H3K27me3 levels (>1-fold compared with WT), and genes with the H3K27me3 enrichment >35-fold compared with input in $Ezh2^{\Delta/\Delta}$ GMPs in B.

may somewhat overestimate the H3K27me3 levels in $Ezh2^{\Delta/\Delta}$ and $Tet2^{KD/KD}$ $Ezh2^{\Delta/\Delta}$ GMPs. However, quantitative ChIP analysis confirmed the trend of ChIP-sequence data (Fig. 9). These results suggest that Ezh1 plays a crucial role in keeping key developmental regulator genes transcriptionally repressed.

## DISCUSSION

In this study, we first demonstrated that the deletion of *Ezh2* confers a growth advantage to HSCs and results in an MDS/MPN-like disease in mice, similar to the depletion of *Tet2*. $Ezh2^{\Delta/\Delta}$ mice developed a lethal MDS/MPN-like disease with myeloproliferative features, including enhanced repopulating capacity of HSCs and extramedullary hematopoiesis in the spleen, and myelodysplastic features, such as anemia accompanied by enhanced apoptosis in erythroblasts and dysplasia in myeloid cells. These findings are compatible with the recurrent inactivation of *EZH2* genes in myelodysplastic disorders and strongly support the tumor suppressor function

Published November 11, 2013



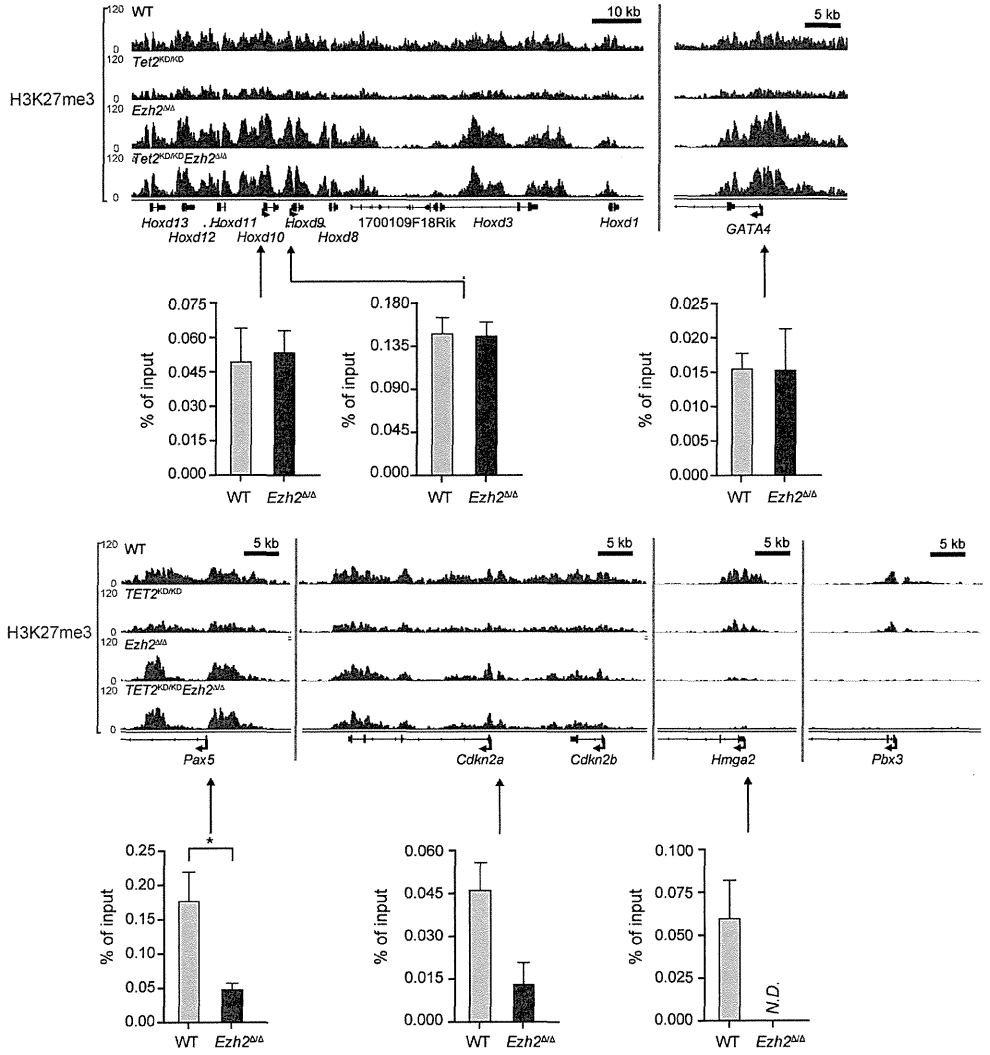


**Figure 9. The levels of H3K27me3 at promoter regions in GMPs.** Visualization of ChIP-seq data of the H3K27me3 levels of several developmental regulator genes (*Hoxd* locus, *Gata4*, and *Pax5*), tumor suppressor genes (*Cdkn2a* and *Cdkn2b*) and oncogenes (*Hmga2* and *Pbx3*) in GMPs from WT, $Tet2^{KD/KD}$, $Ezh2^{\Delta/\Delta}$, and $Tet2^{KD/KD}Ezh2^{\Delta/\Delta}$ mice at 4 mo after transplantation using the Integrative Genomics Viewer (IGV). Schematic diagram of these gene loci indicates their genomic structures. Exons and untranslated regions are demarcated by large and small black boxes, respectively. Data of ChIP analyses at the promoters of selected genes are also depicted. Quantitative ChIP analyses of GMPs from WT and $Ezh2^{\Delta/\Delta}$ mice at 6 mo after transplantation were performed. The relative amounts of immunoprecipitated DNA are depicted as a percentage of input DNA. N.D. indicates not detected. The data are shown as the mean ± SEM for triplicate analyses. Regions amplified from the precipitated DNA by site-specific quantitative PCR are indicated by arrows. *, $P < 0.05$.

of EZH2. Although no mutations have been identified in PRC1 genes, we recently reported that concurrent loss of the PRC1 gene *Bmi1* along with *Ink4a/Arf* in mice causes pathological hematopoiesis that mimics human primary myelofibrosis, a disease categorized as an MPN (Oguro et al., 2012). Together, inactivation of PcG genes could contribute to the pathogenesis of malignant stem cell disorders.

We further demonstrated that inactivating *Ezh2* and *TET2* mutations coexist in 6.7% of patients with myelodysplastic disorders, and concurrent deletion of *Ezh2* and *Tet2* in mice accelerates the development of heterogeneous myelodysplastic disorders including MDS and MDS/MPN. Of note, $Tet2^{KD/KD}Ezh2^{\Delta/\Delta}$ mice showed more advanced myelodysplastic features compared with $Tet2^{KD/KD}$ and $Ezh2^{\Delta/\Delta}$ mice. This is the first study to describe the cooperative effects of the two independent mutations in the pathogenesis of myelodysplastic disorders. Extensive mutation analyses of the myeloid malignancies have revealed that most MDS and MDS/MPN patients have several concurrent genetic mutations, but their pathological meanings remain to be addressed. Our findings highlight the cooperative effects of the independent mutations in the pathogenesis of myelodysplastic disorders. It is assumed that the deregulated gene expression upon concurrent depletion of *Tet2* and *Ezh2* accounts for enhancement in the

Published November 11, 2013



myelodysplastic features, such as dysplasia of myeloid cells, functional defects in neutrophils, and enhanced apoptosis in erythroid cells, although these details require further investigation. On the contrary, *EZH2* mutations are very rare in de novo AML and chronic myeloid leukemia in blastic transformation (CML-BC; Ernst et al., 2010; Chung et al., 2012; Raza and Galili, 2012; Shih et al., 2012), and MDS patients with *EZH2* mutations have much lower risk of transformation to AML compared with those with other gene mutations (Chung et al., 2012; Raza and Galili, 2012; Shih et al., 2012). Indeed, no $Ezh2^{\Delta/\Delta}$ and $Tet2^{KD/KD}Ezh2^{\Delta/\Delta}$ mice developed AML in this study. We and other groups have previously reported that deletion of *Ezh2* largely attenuates the leukemogenecity of AML in a mouse model (Neff et al., 2012; Tanaka et al., 2012). These findings suggest differential roles of EZH2 in AML versus MDS and MDS/MPN.

Although deletion of *Ezh2* results in a drastic reduction in H3K27me3 levels, considerable levels of H3K27me3 are retained. The genes that maintained H3K27me3 levels after loss of Ezh2 largely overlap with the targets of Ezh1 in ES cells, and most of these genes are developmental regulator genes that are marked with bivalent histone domains (Bernstein et al., 2006; Ku et al., 2008). Furthermore, tumor suppressor genes such as *Ink4a/Arf*, a critical PcG target for the maintenance of the self-renewal capacity of HSCs (Oguro et al., 2006), and PcG-targeted developmental regulator genes, such as *Pax5* (Oguro et al., 2010), were kept closely repressed by reduced but significant levels of H3K27me3 modification (Fig. 9). These findings indicate that Ezh1 is capable of repressing developmental regulator genes and tumor suppressor genes, acting to maintain pathological stem cells in the absence of Ezh2. Of interest, Ezh1 was recently reported to maintain HSCs in a slow-cycling, undifferentiated state (Hidalgo et al., 2012). Together, our findings suggest that Ezh1 plays a critical role in pathological stem cells as well as HSCs.

In contrast, several PcG targets became derepressed in $Ezh2^{\Delta/\Delta}$ and $Tet2^{KD/KD}Ezh2^{\Delta/\Delta}$ LSK cells. These included many direct PcG targets that are potential oncogenes, such as *Hmga2*, *Pbx3*, and *Lmo1*. Furthermore, the Myc module, which is active in various cancers, was positively enriched in $Ezh2^{\Delta/\Delta}$ LSK cells and further enriched in MDS/MPN and MDS LSK cells. The derepression of PcG-targeted oncogenes in conjunction with the up-regulation of the Myc module could function as the major drivers in HSCs for the induction of myelodysplastic and myeloproliferative disorders in the absence of Ezh2.

Of interest, Ezh2 knock-in (Ezh2-KI) mice overexpressing *Ezh2* specifically in hematopoietic cells develop MPN (Herrera-Merchan et al., 2012). Ezh2-KI mice show an enhanced HSC activity similarly to $Ezh2^{\Delta/\Delta}$ mice in this study. GSEA showed significant positive enrichment of the Myc module in both $Ezh2^{\Delta/\Delta}$ and Ezh2-KI LSK cells (unpublished data). However, Ezh2-KI mice do not show myelodysplastic features. Apoptosis in LSK cells is suppressed in Ezh2-KI mice but enhanced in $Ezh2^{\Delta/\Delta}$ mice. Ezh2-KI LSK cells show enhanced colony-forming capacity, whereas $Ezh2^{\Delta/\Delta}$ LSK cells show severely compromised proliferation in culture probably due to failure in the transcriptional repression of tumor suppressor genes such as $p19^{Arf}$ (unpublished data), as we have previously reported in transformed myeloid progenitors (Tanaka et al., 2012). These findings clearly discriminate the effects of overexpression and loss/hypomorphism of Ezh2 on hematopoiesis, even though both results in clonal propagation of HSCs.

Finally, the functional cross talk between DNA and histone modifications is an intriguing issue to understand the epigenetics of myeloid malignancies. $Tet2^{KD/KD}Ezh2^{\Delta/\Delta}$ mice developed not only MDS/MPN but also MDS, whereas $Ezh2^{\Delta/\Delta}$ mice developed only MDS/MPN. Moreover, myelodysplastic features were more pronounced in $Tet2^{KD/KD}Ezh2^{\Delta/\Delta}$ mice compared with $Ezh2^{\Delta/\Delta}$ mice. These findings suggest that loss of Ezh2 and Tet2 cooperate to generate a MDS phenotype in mice. However, enhanced apoptosis in the absence of Ezh2 was significantly attenuated in LSK cells, but not in erythroblasts, upon down-regulation of the *Tet2* expression, suggesting an opposing impact of loss of Ezh2 and Tet2 on apoptosis in MDS-initiating hematopoietic stem and progenitor cells.

The understanding of the pathological significance of each somatic gene mutation in myeloid malignancies is just starting to be revealed. Nevertheless, our findings clearly indicate that mouse models, including our own, are capable of faithfully mimicking myelodysplastic disorders and can serve as valuable tools for the analysis of epigenomics of myelodysplastic disorders and preclinical therapeutic studies.

## MATERIALS AND METHODS

**Sequencing analysis of primary samples with MDS and related myeloid neoplasms.** Genomic DNAs from 119 BM samples with MDS and related neoplasms were analyzed for mutations of *TET2*, *IDH1*, *IDH2*, *EZH2*, and *ASXL1* genes by high-throughput sequencing of SureSelect-enriched target exons (Agilent Technologies) according to manufacturer's protocol. Genome-wide copy number lesions were also analyzed using GeneChip SNP-genotyping microarrays (Affymetrix) as previously described (Chen et al., 2008). Allelic imbalances were detected from the allele-specific copy numbers calculated using CNAG/AsCNAR software (http://www.genome.umin.jp; Nannya et al., 2005; Yamamoto et al., 2007). All mutations were confirmed by Sanger-sequencing. All patient samples were appropriately anonymized before the analysis according to the protocol approved by the Ethics Boards of the University of Tokyo.

**Mice and generation of fetal liver chimeras.** $Tet2^{KD/KD}$ and $Ezh2^{fl/fl}$ mice, which had been backcrossed at least eight times onto a C57BL/6 (CD45.2) background, were used (Mochizuki-Kashio et al., 2011; Shide et al., 2012). For conditional deletion of *Ezh2*, the mice were crossed with *Rosa::Cre-ERT* mice (Taconic). C57BL/6 (CD45.2) mice were purchased from Japan SLC. C57BL/6 mice congenic for the Ly5 locus (CD45.1) were purchased from Sankyo-Lab Service. All experiments using the mice were performed in accordance with our institutional guidelines for the use of laboratory animals and approved by the Review Board for animal experiments of Chiba University (approval ID: 25–104). To generate fetal liver chimeras, we intravenously transplanted E14.5 fetal liver from CD45.2 mutant mice (test cells) into 8-wk-old CD45.1 recipients irradiated at a dose of 9.5 Gy. After 1 mo, the recipient mice were injected with 100 µl tamoxifen dissolved in corn oil at a concentration of 10 mg/ml intraperitoneally once a day for 5 consecutive days to induce Cre activity.

**Serial transplantation assay.** 600 CD45.2 LSK cells were sorted from the BM of the primary recipient mice reconstituted with WT, $Tet2^{KD/KD}$, $Ezh2^{\Delta/\Delta}$,

Published November 11, 2013



and $Tet2^{KD/KD}Ezh2^{\Delta/\Delta}$ cells at 4 mo after transplantation and injected into lethally irradiated CD45.1 mice (secondary recipient mice) along with $4 \times 10^5$ BM cells (CD45.1) for competitor cells. For tertiary transplantation, $2 \times 10^6$ whole BM cells taken from the secondary recipient mice 4 mo after transplantation were injected into lethally irradiated CD45.1 mice.

**Western blot analysis of H3K27me3.** Samples were separated by SDS-PAGE, transferred to a PVDF membrane and detected by Western blotting using the following antibodies: anti-H3 (Abcam) and anti-H3K27me3 (Millipore).

**Flow cytometry and antibodies.** mAbs recognizing the following antigens were used in flow cytometry and cell sorting: CD45.2 (104), CD45.1 (A20), Gr-1 (RB6-8C5), CD11b/Mac-1 (M1/70), Ter-119, CD127/IL-7Rα (A7R34), B220 (RA3-6B2), CD4 (L3T4), CD8α (53–6.7), CD117/c-Kit (2B8), Sca-1 (D7), and CD16/32/FcγRII-III (93). The mAbs were purchased from BD, eBioscience, or BioLegend. For Annexin V staining, cells were suspended with 1× Annexin binding buffer (BD) and stained with FITC-Annexin V (BD) according to the manufacturer's protocol. Dead cells were eliminated by staining with 1 μg/ml propidium iodide (Sigma-Aldrich). All flow cytometric analyses and cell sorting were performed on a FACSAria II or FACSCanto II (BD).

**Microarray analysis.** A one-color microarray-based gene expression analysis system (Agilent Technologies) containing 39,429 clones was used (SurePrint G3 Mouse GE 8 × 60K array; Agilent Technologies), according to the manufacturer's instructions. Total RNA was extracted from $5 \times 10^4$ sorted LSK cells or GMPs. A total of 10 ng of total RNA was mixed with spike-in controls using a One Color Spike Mix kit (Agilent Technologies), amplified and labeled with Cyanine 3 using a Quick Amp Labeling kit (Agilent Technologies) according to the manufacturer's instructions, which generated single-color labeled cRNA. A total of 1,650 ng of the labeled cRNA was used for each hybridization. The process of hybridization and washing was performed using a Hi-RPM Gene Expression Hybridization kit (Large; Agilent Technologies) and a Gene Expression Wash Pack (Agilent Technologies), respectively. A DNA microarray scanner (Agilent Technologies) was used for array scanning.

**qRT-PCR.** Total RNA was isolated using TRIZOL LS solution (Invitrogen) and reverse transcribed by the ThermoScript RT-PCR system (Invitrogen) with an oligo-dT primer. Real-time quantitative RT-PCR (qRT-PCR) was performed with an ABI Prism 7300 Thermal Cycler (Applied Biosystems) using FastStart Universal Probe Master (Roche) and the indicated combinations of Universal Probe Library (Roche) and primers listed below.

Primer sequences and probe numbers for real-time RT-PCR (forward/reverse): *Hmga2*, 5′-AAGGCAGCAAAAACAAGAGC-3′/5′-CCGTTTTTCTCCAATGGTCT-3′; *Pbx3*, 5′-GCCTTGGAGCAAACTCACTG-3′/5′-AGATGGAGTTGTTGCGTCCT-3′; *Hprt1*, 5′-TCCTCCTCAGACCGCTTTT-3′/5′-CCTGGTTCATCATCGCTAATC-3′. Primer sequences for manual ChIP analysis at promoter regions: (forward/reverse primer) *Hoxd10*, 5′-TCTCATTGGCTTGGTTGTCA-3′/5′-CAGGAGAGCTGTTGGGAAAG-3′; *Hoxd9*, 5′-TTAAACAACACGCCAAGCTG-3′/5′-AAACCCATCCCTACACACACA-3′; *Gata4*, 5′-ACAGCTCTCTGGTGGCTCTC-3′/5′-AGGTGGTATTCCAGCCCTCT-3′; *Pax5*, 5′-CCACTGGACAATGGCAGTTT-3′/5′-TCCCCCTATCCTCGAACTCT-3′; *Cdkn2a*, 5′-GATGGAGCCCGGACTACAGAAG-3′/5′-CTGTTTCAACGCCCAGCTCTC-3′; *Hmga2*, 5′-AAAACTTGGGCTCCGGGTGCAGA-3′/5′-GGGCGCCCAGCTCAGCTCTAG-3′.

**ChIP assay and ChIP assay coupled with massive parallel sequencing (ChIP-Seq).** GMPs from the BM of recipient mice were cross-linked with 0.5% formaldehyde for 5 min at room temperature, washed three times with PBS, and lysed with RIPA buffer (10 mM Tris, pH 8.0, 140 mM NaCl, 1 mM EDTA, 1% Triton X-100, 0.1% SDS, 0.1% sodium deoxycholate [DOC], and protease inhibitor cocktail) and sonicated for 30 min using a Microson XL2000 Ultrasonic cell disruptor (Misonix). The mean chromatin fragment size after sonication was ~200–300 bp. After centrifugation, the soluble chromatin fraction was recovered, precleared for 1 h at 4°C with a mixture of Protein A– and G–conjugated Dynabeads (Invitrogen) blocked with BSA and salmon (Invitrogen), and then incubated with an anti-H3K27me3 antibody (07–449; Millipore) for 2 h at 4°C. Chromatin was immunoprecipitated overnight at 4°C with antibody-conjugated Dynabeads. The immunoprecipitates were extensively washed with the following combination of wash buffers: high salt RIPA buffer (10 mM Tris, pH 8.0, 500 mM NaCl, 1 mM EDTA, 1% Triton X-100, 0.1% SDS, 0.1% DOC, and protease inhibitor cocktail), LiCl wash buffer (10 mM Tris-HCl, pH 8.0, 250 mM LiCl, 1 mM EDTA, 0.5% NP-40, and 0.5% DOC), and TE buffer (10 mM Tris-HCl, pH 8.0, and 1 mM EDTA. Bound chromatin and input DNA were placed in elution buffer (10 mM Tris-HCl, pH 8.0, 5 mM EDTA, 300 mM NaCl, and 0.5% SDS) and reverse cross-linked. Immunoprecipitated DNA and input DNA were treated with RNase A (Sigma-Aldrich) and proteinase K (Roche), and purified with a QIAquick PCR purification kit (QIAGEN). For ChIP assay, quantitative PCR was performed with an ABI prism 7300 Thermal Cycler using SYBR Premix Ex Taq II (Takara Bio). The primer sequences are listed above. For ChIP-Seq, immunoprecipitated DNA and input samples were then prepared using ChIP-Seq Sample Prep kit (Illumina). Adaptor-ligated DNA fragments were size fractionated by 12% acrylamide gel, and the 170- to 250-bp fraction was recovered. DNA thus obtained was amplified by 18 cycles of PCR. 1 ng DNA was used for the sequencing reaction of the GAIIx (Illumina), according to the manufacturer's instructions. A total of 170,000–250,000 clusters were generated per tile, and 36 cycles of the sequencing reactions were performed. Short-read sequences were aligned to the mouse genome sequences (mm9 from University of California, Santa Cruz Genome Browser; http://genome.ucsc.edu/) using the Eland program. Sequences allowing no more than two mismatches per sequence were used for the analysis. The ChIP-Seq signal was quantified as total number of reads per million. To enumerate genes with H3K27me3 modification, genes with cumulative tag numbers in the region 5.0 kb upstream of the TSS to 0.5 kb downstream of the TSS greater than twofold was selected.

**Statistical analysis.** Heat map was drawn by Matrix2png (Pavlidis and Noble, 2003). Statistical tests were performed using Prism (version 5; GraphPad Software). For analysis of survival curves, log rank (Mantel-Cox) test was performed.

**Deposition of the data.** Microarray and ChIP-sequence data were deposited in Gene Expression Omnibus (accession no. GSE42666) and DNA Data Bank of Japan (DDBJ, accession no. DRA000485-488), respectively.

**Online supplemental material.** Table S1 lists the gene mutations and abnormalities in chromosome 7 in patient samples. Table S2 provides the detailed hematological characteristics of diseased mice. Table S3 lists the potential oncogenes of direct PcG targets derepressed in the absence of Ezh2. Table S4 lists the genes with a fold enrichment of H3K27me3 >35 compared with input in *Ezh2*-deficient GMPs. Online supplemental material is available at http://www.jem.org/cgi/content/full/jem.20131144/DC1.

We thank Terumi Horiuchi for data mining of the ChIP-seq analysis and Kazue Imai for assistance on statistical analysis.

This work was supported in part by Grants-in-aid for Scientific Research (#24249054 and #221S0002), Scientific Research on Innovative Areas "Genome Science" (#221S0002) and the Global COE Program (Global Center for Education and Research in Immune System Regulation and Treatment) from MEXT, Japan, a Grant-in-aid for Core Research for Evolutional Science and Technology (CREST) from the Japan Science and Technology Corporation (JST), and grants from the Takeda Science Foundation, the Uehara Memorial Foundation, and the Tokyo Biochemical Research Foundation.

The authors have no competing financial interests to declare.

**Submitted: 1 June 2013**
**Accepted: 15 October 2013**

Published November 11, 2013

JEM

## REFERENCES

Abdel-Wahab, O., A. Pardanani, J. Patel, M. Wadleigh, T. Lasho, A. Heguy, M. Beran, D.G. Gilliland, R.L. Levine, and A. Tefferi. 2011. Concomitant analysis of EZH2 and ASXL1 mutations in myelofibrosis, chronic myelomonocytic leukemia and blast-phase myeloproliferative neoplasms. *Leukemia.* 25:1200–1202. http://dx.doi.org/10.1038/leu.2011.58

Abdel-Wahab, O., M. Adli, L.M. LaFave, J. Gao, T. Hricik, A.H. Shih, S. Pandey, J.P. Patel, Y.R. Chung, R. Koche, et al. 2012. ASXL1 mutations promote myeloid transformation through loss of PRC2-mediated gene repression. *Cancer Cell.* 22:180–193. http://dx.doi.org/10.1016/j.ccr.2012.06.032

Bejar, R., K. Stevenson, O. Abdel-Wahab, N. Galili, B. Nilsson, G. Garcia-Manero, H. Kantarjian, A. Raza, R.L. Levine, D. Neuberg, and B.L. Ebert. 2011. Clinical effect of point mutations in myelodysplastic syndromes. *N. Engl. J. Med.* 364:2496–2506. http://dx.doi.org/10.1056/NEJMoa1013343

Bernstein, B.E., T.S. Mikkelsen, X. Xie, M. Kamal, D.J. Huebert, J. Cuff, B. Fry, A. Meissner, M. Wernig, K. Plath, et al. 2006. A bivalent chromatin structure marks key developmental genes in embryonic stem cells. *Cell.* 125:315–326. http://dx.doi.org/10.1016/j.cell.2006.02.041

Challen, G.A., D. Sun, M. Jeong, M. Luo, J. Jelinek, J.S. Berg, C. Bock, A. Vasanthakumar, H. Gu, Y. Xi, et al. 2012. Dnmt3a is essential for hematopoietic stem cell differentiation. *Nat. Genet.* 44:23–31. http://dx.doi.org/10.1038/ng.1009

Chen, Y., J. Takita, Y.L. Choi, M. Kato, M. Ohira, M. Sanada, L. Wang, M. Soda, A. Kikuchi, T. Igarashi, et al. 2008. Oncogenic mutations of ALK kinase in neuroblastoma. *Nature.* 455:971–974. http://dx.doi.org/10.1038/nature07399

Chung, Y.R., E. Schatoff, and O. Abdel-Wahab. 2012. Epigenetic alterations in hematopoietic malignancies. *Int. J. Hematol.* 96:413–427. http://dx.doi.org/10.1007/s12185-012-1181-z

Dey, A., D. Seshasayee, R. Noubade, D.M. French, J. Liu, M.S. Chaurushiya, D.S. Kirkpatrick, V.C. Pham, J.R. Lill, C.E. Bakalarski, et al. 2012. Loss of the tumor suppressor BAP1 causes myeloid transformation. *Science.* 337:1541–1546. http://dx.doi.org/10.1126/science.1221711

Ernst, T., A.J. Chase, J. Score, C.E. Hidalgo-Curtis, C. Bryant, A.V. Jones, K. Waghorn, K. Zoi, F.M. Ross, A. Reiter, et al. 2010. Inactivating mutations of the histone methyltransferase gene EZH2 in myeloid disorders. *Nat. Genet.* 42:722–726. http://dx.doi.org/10.1038/ng.621

Herrera-Merchan, A., L. Arranz, J.M. Ligos, A. de Molina, O. Dominguez, and S. Gonzalez. 2012. Ectopic expression of the histone methyltransferase Ezh2 in haematopoietic stem cells causes myeloproliferative disease. *Nat Commun.* 3:623. http://dx.doi.org/10.1038/ncomms1623

Hidalgo, I., A. Herrera-Merchan, J.M. Ligos, L. Carramolino, J. Nuñez, F. Martinez, O. Dominguez, M. Torres, and S. Gonzalez. 2012. Ezh1 is required for hematopoietic stem cell maintenance and prevents senescence-like cell cycle arrest. *Cell Stem Cell.* 11:649–662. http://dx.doi.org/10.1016/j.stem.2012.08.001

Kim, J., A.J. Woo, J. Chu, J.W. Snow, Y. Fujiwara, C.G. Kim, A.B. Cantor, and S.H. Orkin. 2010. A Myc network accounts for similarities between embryonic stem and cancer cell transcription programs. *Cell.* 143:313–324. http://dx.doi.org/10.1016/j.cell.2010.09.010

Ko, M., Y. Huang, A.M. Jankowska, U.J. Pape, M. Tahiliani, H.S. Bandukwala, J. An, E.D. Lamperti, K.P. Koh, R. Ganetzky, et al. 2010. Impaired hydroxylation of 5-methylcytosine in myeloid cancers with mutant TET2. *Nature.* 468:839–843. http://dx.doi.org/10.1038/nature09586

Konuma, T., H. Oguro, and A. Iwama. 2010. Role of the polycomb group proteins in hematopoietic stem cells. *Dev. Growth Differ.* 52:505–516. http://dx.doi.org/10.1111/j.1440-169X.2010.01191.x

Ku, M., R.P. Koche, E. Rheinbay, E.M. Mendenhall, M. Endoh, T.S. Mikkelsen, A. Presser, C. Nusbaum, X. Xie, A.S. Chi, et al. 2008. Genomewide analysis of PRC1 and PRC2 occupancy identifies two classes of bivalent domains. *PLoS Genet.* 4:e1000242. http://dx.doi.org/10.1371/journal.pgen.1000242

Li, Z., Z. Zhang, Y. Li, S. Arnovitz, P. Chen, H. Huang, X. Jiang, G.M. Hong, R.B. Kunjamma, H. Ren, et al. 2013. PBX3 is an important cofactor of HOXA9 in leukemogenesis. *Blood.* 121:1422–1431 http://dx.doi.org/10.1182/blood-2012-07-442004

Mochizuki-Kashio, M., Y. Mishima, S. Miyagi, M. Negishi, A. Saraya, T. Konuma, J. Shinga, H. Koseki, and A. Iwama. 2011. Dependency on the polycomb gene Ezh2 distinguishes fetal from adult hematopoietic stem cells. *Blood.* 118:6553–6561. http://dx.doi.org/10.1182/blood-2011-03-340554

Moran-Crusio, K., L. Reavie, A. Shih, O. Abdel-Wahab, D. Ndiaye-Lobry, C. Lobry, M.E. Figueroa, A. Vasanthakumar, J. Patel, X. Zhao, et al. 2011. Tet2 loss leads to increased hematopoietic stem cell self-renewal and myeloid transformation. *Cancer Cell.* 20:11–24. http://dx.doi.org/10.1016/j.ccr.2011.06.001

Morin, R.D., N.A. Johnson, T.M. Severson, A.J. Mungall, J. An, R. Goya, J.E. Paul, M. Boyle, B.W. Woolcock, F. Kuchenbauer, et al. 2010. Somatic mutations altering EZH2 (Tyr641) in follicular and diffuse large B-cell lymphomas of germinal-center origin. *Nat. Genet.* 42:181–185. http://dx.doi.org/10.1038/ng.518

Nannya, Y., M. Sanada, K. Nakazaki, N. Hosoya, L. Wang, A. Hangaishi, M. Kurokawa, S. Chiba, D.K. Bailey, G.C. Kennedy, and S. Ogawa. 2005. A robust algorithm for copy number detection using high-density oligonucleotide single nucleotide polymorphism genotyping arrays. *Cancer Res.* 65:6071–6079. http://dx.doi.org/10.1158/0008-5472.CAN-05-0465

Neff, T., A.U. Sinha, M.J. Kluk, N. Zhu, M.H. Khattab, L. Stein, H. Xie, S.H. Orkin, and S.A. Armstrong. 2012. Polycomb repressive complex 2 is required for MLL-AF9 leukemia. *Proc. Natl. Acad. Sci. USA.* 109:5028–5033. http://dx.doi.org/10.1073/pnas.1202258109

Nikoloski, G., S.M. Langemeijer, R.P. Kuiper, R. Knops, M. Massop, E.R. Tönnissen, A. van der Heijden, T.N. Scheele, P. Vandenberghe, T. de Witte, et al. 2010. Somatic mutations of the histone methyltransferase gene EZH2 in myelodysplastic syndromes. *Nat. Genet.* 42:665–667. http://dx.doi.org/10.1038/ng.620

Oguro, H., A. Iwama, Y. Morita, T. Kamijo, M. van Lohuizen, and H. Nakauchi. 2006. Differential impact of Ink4a and Arf on hematopoietic stem cells and their bone marrow microenvironment in Bmi1-deficient mice. *J. Exp. Med.* 203:2247–2253. http://dx.doi.org/10.1084/jem.20052477

Oguro, H., J. Yuan, H. Ichikawa, T. Ikawa, S. Yamazaki, H. Kawamoto, H. Nakauchi, and A. Iwama. 2010. Poised lineage specification in multipotential hematopoietic stem and progenitor cells by the polycomb protein Bmi1. *Cell Stem Cell.* 6:279–286. http://dx.doi.org/10.1016/j.stem.2010.01.005

Oguro, H., J. Yuan, S. Tanaka, S. Miyagi, M. Mochizuki-Kashio, H. Ichikawa, S. Yamazaki, H. Koseki, H. Nakauchi, and A. Iwama. 2012. Lethal myelofibrosis induced by Bmi1-deficient hematopoietic cells unveils a tumor suppressor function of the polycomb group genes. *J. Exp. Med.* 209:445–454. http://dx.doi.org/10.1084/jem.20111709

Pavlidis, P., and W.S. Noble. 2003. Matrix2png: a utility for visualizing matrix data. *Bioinformatics.* 19:295–296. http://dx.doi.org/10.1093/bioinformatics/19.2.295

Pruitt, K.D., T. Tatusova, and D.R. Maglott. 2007. NCBI reference sequences (RefSeq): a curated non-redundant sequence database of genomes, transcripts and proteins. *Nucleic Acids Res.* 35:D61–D65. http://dx.doi.org/10.1093/nar/gkl842

Raza, A., and N. Galili. 2012. The genetic basis of phenotypic heterogeneity in myelodysplastic syndromes. *Nat. Rev. Cancer.* 12:849–859. http://dx.doi.org/10.1038/nrc3321

Sasaki, M., C.B. Knobbe, J.C. Munger, E.F. Lind, D. Brenner, A. Brüstle, I.S. Harris, R. Holmes, A. Wakeham, J. Haight, et al. 2012. IDH1(R132H) mutation increases murine haematopoietic progenitors and alters epigenetics. *Nature.* 488:656–659. http://dx.doi.org/10.1038/nature11323

Sauvageau, M., and G. Sauvageau. 2010. Polycomb group proteins: multi-faceted regulators of somatic stem cells and cancer. *Cell Stem Cell.* 7:299–313. http://dx.doi.org/10.1016/j.stem.2010.08.002

Shen, X., Y. Liu, Y.J. Hsu, Y. Fujiwara, J. Kim, X. Mao, G.C. Yuan, and S.H. Orkin. 2008. EZH1 mediates methylation on histone H3 lysine 27 and complements EZH2 in maintaining stem cell identity and executing pluripotency. *Mol. Cell.* 32:491–502. http://dx.doi.org/10.1016/j.molcel.2008.10.016

Shide, K., T. Kameda, H. Shimoda, T. Yamaji, H. Abe, A. Kamiunten, M. Sekine, T. Hidaka, K. Katayose, Y. Kubuki, et al. 2012. TET2 is essential for survival and hematopoietic stem cell homeostasis. *Leukemia.* 26:2216–2223. http://dx.doi.org/10.1038/leu.2012.94

Published November 11, 2013



Shih, A.H., O. Abdel-Wahab, J.P. Patel, and R.L. Levine. 2012. The role of mutations in epigenetic regulators in myeloid malignancies. *Nat. Rev. Cancer.* 12:599–612. http://dx.doi.org/10.1038/nrc3343

Subramanian, A., P. Tamayo, V.K. Mootha, S. Mukherjee, B.L. Ebert, M.A. Gillette, A. Paulovich, S.L. Pomeroy, T.R. Golub, E.S. Lander, and J.P. Mesirov. 2005. Gene set enrichment analysis: a knowledge-based approach for interpreting genome-wide expression profiles. *Proc. Natl. Acad. Sci. USA.* 102:15545–15550. http://dx.doi.org/10.1073/pnas.0506580102

Tanaka, S., S. Miyagi, G. Sashida, T. Chiba, J. Yuan, M. Mochizuki-Kashio, Y. Suzuki, S. Sugano, C. Nakaseko, K. Yokote, et al. 2012. Ezh2 augments leukemogenicity by reinforcing differentiation blockage in acute myeloid leukemia. *Blood.* 120:1107–1117. http://dx.doi.org/10.1182/blood-2011-11-394932

Tremblay, M., C.S. Tremblay, S. Herblot, P.D. Aplan, J. Hébert, C. Perreault, and T. Hoang. 2010. Modeling T-cell acute lymphoblastic leukemia induced by the SCL and LMO1 oncogenes. *Genes Dev.* 24:1093–1105. http://dx.doi.org/10.1101/gad.1897910

Yamamoto, G., Y. Nannya, M. Kato, M. Sanada, R.L. Levine, N. Kawamata, A. Hangaishi, M. Kurokawa, S. Chiba, D.G. Gilliland, et al. 2007. Highly sensitive method for genomewide detection of allelic composition in nonpaired, primary tumor specimens by use of affymetrix single-nucleotide-polymorphism genotyping microarrays. *Am. J. Hum. Genet.* 81:114–126. http://dx.doi.org/10.1086/518809

*Cytotherapy*, 2013; 15: 255–262

International Society for Cellular Therapy ISCT®

**ORIGINAL PAPERS**

# Current practices and prospects for standardization of the hematopoietic colony-forming unit assay: a report by the cellular therapy team of the Biomedical Excellence for Safer Transfusion (BEST) Collaborative

DERWOOD PAMPHILON[1], EILEEN SELOGIE[6,14], DAVID MCKENNA[2], JOSE A. CANCELAS-PERES[3], ZBIGNIEW M. SZCZEPIORKOWSKI[4], RON SACHER[5], JOHN McMANNIS[6], HERMANN EICHLER[7], HENK GARRITSEN[8], MINOKO TAKANASHI[9], LEO VAN DE WATERING[10], DAVID STRONCEK[11] & JO-ANNA REEMS[12,13]

[1]*NHS Blood and Transplant North Bristol Park, Filton, UK,* [2]*Universtiy of Minnesota, St Paul, Minnesota, USA,* [3]*Hoxworth Blood Center, Cincinnati, Ohio, USA,* [4]*Dartmouth-Hitchcock Medical Center, Lebanon, New Hampshire, USA,* [5]*Hoxworth Blood Center, Cincinnati, Ohio, USA,* [6]*University of Texas, M.D. Anderson Cancer Center, Houston, Texas,* [7]*Institute of Clinical Hemostaseology and Transfusion Medicine, Saarland University Hospital, Homburg/Saar, Germany,* [8]*Staedtisches Klinikum Braunschweig gGMbH, Braunschweig, Germany,* [9]*Japanese Red Cross Kanto-Koshinetsu block Blood Centre, Tokyo, Japan,* [10]*LUMC Jon J. van Rood Center for Clinical Transfusion Research, Leiden, Netherlands,* [11]*National Institutes of Health, Bethesda, Maryland, USA,* [12]*Puget Sound Blood Center and* [13]*University of Washington, Seattle, Washington, USA, and* [14]*ENet Answers, Manhattan Beach, CA, USA*

**Abstract**

*Background aims.* Wide acceptance of the colony-forming unit (CFU) assay as a reliable potency test for stem cell products is hindered by poor inter-laboratory reproducibility. The goal of this study was to ascertain current laboratory practices for performing the CFU assay with an eye towards identifying practices that could be standardized to improve overall reproducibility. *Methods.* A survey to evaluate current laboratory practices for performing CFU assays was designed and internationally distributed. *Results.* There were 105 respondents to the survey, of whom 68% performed CFU assays. Most survey recipients specified that an automated rather than a manual cell count was performed on pre-diluted aliquots of stem cell products. Viability testing methods employed various stains, and when multiple sites used the same viability stain, the methods differed. Cell phenotype used to prepare working cell suspensions for inoculating the CFU assay differed among sites. Most respondents scored CFU assays at 14–16 days of incubation, but culture plates were read with various microscopes. Of 57 respondents, 42% had not performed a validation study or established assay linearity. Only 63% of laboratories had criteria for determining if a plate was overgrown with colonies. *Conclusions.* Survey results revealed inconsistent inter-laboratory practices for performing the CFU assay. The relatively low number of centers with validated CFU assays raises concerns about assay accuracy and emphasizes a need to establish central standards. The survey results shed light on numerous steps of the methodology that could be targeted for standardization across laboratories.

**Key Words:** *colony-forming-units, hematopoietic, hematopoietic progenitor cells, potency test*

## Introduction

Functional analysis of hematopoietic progenitor cell (HPC) products is critical for comparative selection of the highest quality stem cell product for a transplant recipient. However, the selection of stem cell products for transplantation is typically based primarily on non-functional cellular parameters such as total nucleated cell (TNC) counts and cellular immunophenotypes (e.g., $CD34^+$ cell counts). Although these surrogate assays have demonstrated good inverse correlations

Correspondence: **Jo-Anna Reems**, PhD, MT(ASCP)SBB, University of Utah, 676 Arapeen Drive, Suite 300, Salt Lake City, UT 84108, USA. E-mail: joanna.reems@hsc.utah.edu

*(Received 9 July 2012; accepted 11 November 2012)*

ISSN 1465-3249 
http://dx.doi.org/10.1016/j.jcyt.2012.11.013